Earth Syst. Sci. Data Discuss., doi:10.5194/essd-2017-1, 2017
Manuscript under review for journal Earth Syst. Sci. Data
Discussion started: 10 February 2017

Open Access Earth System Science Data Discussions

The Global SMOS Level 3 daily soil moisture and brightness temperature maps

Ahmad Al Bitar[1,2], Arnaud Mialon[1,2], Yann H. Kerr[1,3], François Cabot[1,3], Philippe Richaume[1], Elsa Jacquette[3], Arnaud Quesney[4], Ali Mahmoodi[1], Stéphane Tarot[5], Marie Parrens[1], Amen Al-Yaari[6], Thierry Pellarin[7], Nemesio Rodriguez-Fernandez [1], Jean-Pierre Wigneron[6]

[1] Centre d'Etudes Spatiales de la Biosphère, Université de Toulouse, CNES/CNRS/IRD/UPS, Toulouse, France.
[2] Centre National de Recherche Scientifique, Paris, France.
[3] Centre National d'Etudes Spatiales, Paris, France.
[4] CapGemini Sud, 109 Avenue du Général Eisenhower, 31000 Toulouse, France.
[5] IFremer, BP 70, 29280 Plouzane, France.
[6] INRA, UMR1391 ISPA, Villenave d'Ornon, France.
[7] IGE, University Grenoble Alpes, CNRS/G-INP/IRD/UGA, Grenoble, France.

Correspondence to: Ahmad Al Bitar (ahmad.albitar@cesbio.cnes.fr)

Keywords: soil moisture, SMOS, L-band, SMAP, Multi-orbit, microwave, retrieval algorithm

Abstract: The objective of this paper is to present the multi-orbit (MO) surface Soil Moisture (SM) and angle binned Brightness Temperature (TB) products for the SMOS (Soil Moisture and Ocean Salinity) mission based on the a new multi-orbit algorithm. The Level 3 algorithm at CATDS (Centre de Traitement Aval des Données SMOS) makes use of multi-orbit (multi-revisits) retrieval to enhance the robustness and quality of SM retrievals. The motivation of the approach is to make use of the temporal auto-correlation of the vegetation optical depth (VOD) to enhance the retrievals when an acquisition occurs at the border of the swath. The retrieval algorithm is implemented in a unique operational processor delivering multiple parameters (e.g. SM and VOD) using angular signatures, dual polarization and multiple revisits. A subsidiary angle binned TB product is provided. In this study the L3 TB V300 product is showcased and compared to SMAP (Soil Moisture Active Passive) TB. The L3 SM V300 product is compared to the single-orbit (SO) retrievals from Level 2 SM processor from ESA (European Space Agency) with aligned

Earth Syst. Sci. Data Discuss., doi:10.5194/essd-2017-1, 2017
Manuscript under review for journal Earth Syst. Sci. Data
Discussion started: 10 February 2017

configuration. The advantages and drawbacks of the Level 3 SM product (L3SM) product are discussed. The comparison is done at global scale between the two datasets and at local scale with respect to *in situ* data from AMMA-CATCH and USDA-ARS WATERSHEDS networks. The results obtained from the global analysis show that the MO implementation enhances the number of retrievals up to 9 % over certain areas. The comparison with the *in situ* data shows that the increase of the number of retrievals does not come with a decrease of quality. But rather at the expense of an increased lag of product availability from 6 hours to 3.5 days which can be a limiting factor for forecast applications like flood forecast but reasonable for drought monitoring and climate change studies. The SMOS L3 soil moisture and L3 brightness temperature products are delivered using an open licence and free of charge by CATDS (http://www.catds.fr).

Abbreviations

ARS	Agricultural Research Service
AMMA	Analyse Multidisciplinaire de la Mousson
AMSR-E	Advanced Microwave Scanning Radiometer - Earth Observing System
ASCAT	Advanced Scatterometer
CATDS	Centre Aval de Traitement des Données SMOS
CNES	Centre National d'Etudes Spatiales
CCI	Climate Change Initiative
CDTI	Centro para el Desarrollo Tecnológico Industrial
DPGS	Data Processing Ground Segment
EASE-Grid	Equal-Area Scalable Earth Grid
ECMWF	European Centre for Medium-Range Weather Forecasts
ECV	Essential Climate Variables
EO	Earth Observation
ESA	European Space Agency
IFREMER	Institut Français de Recherche pour l'Exploitation de la Mer
ISEA	Icosahedral Snyder Equal Area
L-MEB	L-band Microwave Emission of the Biosphere
MO	Multi Orbit
NASA	National Aeronautics and Space Administration (U.S.A.)
SM	Soil Moisture
SMAP	Soil Moisture Active and Passive

Earth Syst. Sci. Data Discuss., doi:10.5194/essd-2017-1, 2017
Manuscript under review for journal Earth Syst. Sci. Data
Discussion started: 10 February 2017

Open Access Earth System Science Data Discussions

60	SMOS	Soil Moisture and Ocean Salinity
61	SMUDP	Soil Moisture User Data Product
62	SO	Single Orbit
63	TOA	Top of Atmosphere
64	USDA	United States Department of Agriculture
65	VOD	Vegetation Optical Depth

Earth Syst. Sci. Data Discuss., doi:10.5194/essd-2017-1, 2017
Manuscript under review for journal Earth Syst. Sci. Data
Discussion started: 10 February 2017

Open Access Earth System Science Data Discussions

1. Introduction

Surface Soil Moisture (SM) is a control physical parameter for many hydrological processes like infiltration, runoff, precipitation and evaporation (Koster et al., 2004). Estimates of SM are needed for many applications concerned with monitoring droughts (Keyantash & Dracup, 2002), floods (Brocca et al., 2010, Lievens et al., 2015), weather forecast (Drusch, 2007, de Rosnay et al., 2013), climate (Jung et al. 2010), and agriculture (Guérif & Duke, 2000). It is identified among the 50 Essential Climate Variables (ECV) for the Global Climate Observing Systems (GCOS). It has been also selected for the creation of decadal time series from remote sensing in the European Space Agency (ESA) Climate Change Initiative (CCI) project (Hollmann et al., 2013).

SM can be obtained from several Earth Observation (EO) techniques ranging from visible to microwave using active (Ulaby et al., 1996) and passive (Kerr & Njoku. 1990) instruments. Retrieval of SM from microwave sensors is a challenging exercise because features like surface heterogeneity (water surfaces, land use), vegetation cover (vegetation density and distribution), climatic conditions (freezing, snow), acquisition configurations (angle, frequency, polarisation), and topography (multiple scattering) need to be carefully considered while upscaling to the sensor coarse resolution. Several approaches like regression models (Njoku et al., 2003, Wigneron et al., 2004 and Saleh et al., 2006), statistical and contextual methods (Verhoest et al., 1998), neural networks (Liu et al., 2002, Rodriguez-Fernandez et al., 2015) and radiative transfer based approaches (Kerr & Njoku, 1990, Wigneron et al., 2007, Owe et al., 2008, O'Neill et al., 2013) have been developed to retrieve SM based on the sensor frequency, acquisition modes and richness of information (multi angular, full polarization, a[illegible]). The Soil Moisture and Ocean Salinity (SMOS) mission of ESA (Kerr et al., 2001, 2010) with contributions from Centre National d'Etudes Spatiales (CNES) in France and Centro para el Desarrollo Tecnológico Industrial (CDTI) in Spain is the first earth observation mission dedicated for SM mapping. The SMOS Level 2 (L2) SM retrieval algorithm (Kerr et al., 2012) uses the L-band Microwave Emission of the Biosphere (L-MEB) radiative transfer model (Wigneron et al., 2007) as a forward operator in association with the Levenberg-Marquardt optimization algorithm to retrieve physical parameters, mainly SM and VOD.

Earth Syst. Sci. Data Discuss., doi:10.5194/essd-2017-1, 2017
Manuscript under review for journal Earth Syst. Sci. Data
Discussion started: 10 February 2017

The L-MEB radiative transfer model is based on the optical depth single scattering albedo (τ–ω) model (Mo et al., 1982) combined to specific parameterisations to take into account the impact of vegetation and soil roughness on polarization mixing and angular signature. The Soil Moisture Active Passive (SMAP) mission, launched by NASA on January 2015 delivers observations on a fixed (40°) incidence angle (Entekhabi et al. 2010). The SMAP soil moisture processor currently relies on a Single Channel Algorithm (SCA) (O'Neill et al., 2012) for its main product. This algorithm uses a forced vegetation optical thickness in a single-orbit configuration. Miernecki et al. (2015) presented a review and a comparison of the different retrieval approaches for L-Band microwave from EO missions (SMOS, SMAP, AQUARIUS).

Passive microwave sensors have a high revisit frequency: 1 day for Advanced Microwave Scanning Radiometer - Earth Observing System (AMSR-E) (Njoku & Entekhabi , 1996), and 2-3 days for SMOS and SMAP. In this study the multi-orbit (MO) , multi-angular and dual channel (H/V) operational retrieval algorithm implemented at the CATDS (Centre Aval de Traitement des Données SMOS) by Centre National d'Etudes Spatiales (CNES) is presented. Retrieval using temporal series is becoming increasingly common in operational EO retrieval algorithms for optical and to some extent microwave technologies. Some examples in the optical domain are the correction of aerosols impact for visible images (Hagolle et al., 2008, 2015), the cloud detection (Hagolle et al., 2010) and the use of multiple revisits for land cover classification (Inglada & Mercier, 2007). The previous methodologies are being implemented for high-end level 2-A and level 3 products for the Copernicus Sentinel-2 mission. The use of multiple revisits in the radar community is a standard approach. The SM retrievals from ERS, Advanced Scatterometer (ASCAT), RADARSAT-2 and Sentinel-1 are based on a change detection algorithm (Wagner et al., 1999, 2013; Naeimi et al., 2009). Similarly, Mattia et al. (2006) introduced a priori surface parameters and multi-temporal Synthetic Aperture Radar (SAR) data to remove the impact of vegetation and soil roughness in SM retrieval from SAR. Recently a generalization of change detection to multiple regression using Cumulative Distribution Function (CDF) transformations was applied to RADARSAT-2 time series data and validated over the Berambadi watershed, South India (Tomer et al., 2015). In microwave radiometry, Konings et al. (2016) presented a time series retrieval of vegetation optical depth based on AQUARIUS L-Band acquisitions.

Earth Syst. Sci. Data Discuss., doi:10.5194/essd-2017-1, 2017
Manuscript under review for journal Earth Syst. Sci. Data
Discussion started: 10 February 2017

Here a detailed presentation of the products and retrieval algorithm and an inter-comparison between the SMOS SO (Single orbit) and the SMOS MO (Multi-orbit) operational products is done. More specifically, the objective of this paper is to present the daily L3 SM and TB V300 products and associated algorithms and to compare the SMOS MO level 3 retrievals to the level 2 single-orbit operational retrievals that are were obtained using V600 L1 ESA-SMOS products. Since the SMOS mission launch in November 2009, this is the first reprocessing to have an aligned version of the processors from Level 1 up to Level 3 enabling a direct comparison of the products. In the next sections, the multi-orbit retrieval SM algorithm and angle binned TB are presented. The datasets used for the assessment, the results of the comparison and conclusions are presented.

2. The CATDS Level-3 soil moisture processor

2.1 Algorithm overview

The Level-3 SM (L3SM) processor is a set of several algorithms. The forward model in L3SM uses the same physically based forward models as the ESA SMOS Level 2 SM processor, but in a MO retrieval context. A short summary of the main features of this processor is provided hereby, a detailed description is provided in (Kerr et al. 2012). The SMOS L2 retrieval can be divided into two main components:

1) The first component is a physical model that computes TB at the antenna reference frame forced by ancillary data (land classification, soil properties) and physical parameters (skin or near-surface temperature and soil temperature).. The selected physical model for the SMOS mission is L-MEB from Wigneron et al. (2007). The main features of the L-MEB physical model implementation in the SMOS operational processor are:

- Effective scattering albedo is considered.
- SM and VOD are jointly retrieved over nominal (bare soil and low vegetation) surfaces using angular signature information.
- Dual polarization is used. Full polarisation data is only used to take into account the Faraday rotation and geometric rotation to transform modelled TB from the Top Of Atmosphere (TOA) to the antenna reference frame.

Earth Syst. Sci. Data Discuss., doi:10.5194/essd-2017-1, 2017
Manuscript under review for journal Earth Syst. Sci. Data
Discussion started: 10 February 2017

- The mean antenna pattern (Kerr et al., 2012) is used in the iterative retrieval algorithm. The mean weighting function expresses the average contributions for all angular acquisitions. The -3 dB footprints is about km in radius. This corresponds to the nominal resolution of the synthetic aperture. Also this corresponds to of the signal if a homogeneous surface is considered (Al Bitar et al., 2012).
- Surface heterogeneity is considered through aggregated TB contributions from 4 × 4 km² surface units. The contributions are then convoluted by the mean antenna pattern. A total area of 125 × 125 km² is considered at each retrieval node to compute the total ributions.
- Dynamic changes in surface state (freezing, rainfall…) are considered through the use of ancillary weather data from ECMWF (European Centre for Medium-Range Weather Forecasts) reanalysis products.

Since the mission launch many improvements have been implemented in the operational processing model see for instance the improved parametrization of the forest albedo in Rahmoune et al., (2014) or the choice of dielectric mixing models in Mialon et al., (2015).

2) The second component of the retrieval algorithm is an iterative optimization scheme that minimises a Bayesian cost function constructed from the observed and the modelled TBs in order to retrieve the sical parameter values. Pre-processing and post-processing steps are implemented to filter the input and output data for undesired effects, like the decrease of quality due to spatial sampling or Radio Frequency Interferences (RFI) (Oliva et al., 2012, Richaume et al., 2014).

The physical approach at Level-3 MO is the same as that of Level-2 SO. In fact the core processing uses the same implementation of the L-MEB radiative transfer model. The main difference in Level-3 is the use of several orbits, rather than one, to retrieve SM and VOD. This has an impact first on the post-processing steps for selecting the orbits and second on the optimization scheme to retrieve the parameters. Since the Level-2 retrieval is a multi-parameter retrieval, the Level-3 is thus a multi-orbit multi-parameter retrieval. The reasons that motivated the use of the MO approach are the following:

Earth Syst. Sci. Data Discuss., doi:10.5194/essd-2017-1, 2017
Manuscript under review for journal Earth Syst. Sci. Data
Discussion started: 10 February 2017

- The angular sampling and radiometric accuracy at the border of the swath is reduced. Figure 1 shows the cumulative number of records (TB_X, TB_Y, TB_{XY}) for several descending orbits. The asterisk in the images represents the same location in La Plata region, South-America. The reddish region observed on 18th, 20th and 23rd of May 2010 shows the decrease of number of TB measurements during the instrument calibration phases. But most important is the smaller number of TB measurements (35) on the same location observed on the 21th of May image. A low number of TB measurements spanning a narrow range of incidence angles can make the iterative estimation of SM and VOD to fail. The use of MO can help improving the number of successful retrievals at the border.

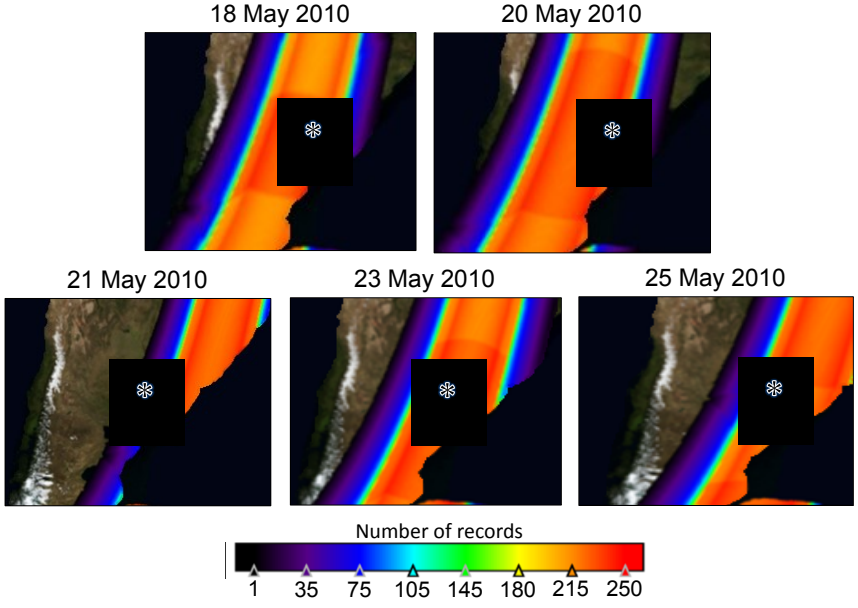

Figure 1 - Number of TB records across the swath for a period of 8 days - from 18 May 2010 to 25 May 2010 - over the area of La Plata Argentina.

- The VOD is expected to vary slowly in time and thus to be highly correlated between two consecutive ascending or descending orbits or over short period of time (few days). In fact at L-band the VOD is mainly correlated to vegetation water content (Jackson & Schmugge, [illegible]).

Earth Syst. Sci. Data Discuss., doi:10.5194/essd-2017-1, 2017
Manuscript under review for journal Earth Syst. Sci. Data
Discussion started: 10 February 2017

Other general motivations for Level-3 products are to provide a global gridded product, in contrast to swath based products and to provide fixed angle binned TB products. The 25 km Equal-Area Scalable Earth Grid version 2.0 (EASE-Grid 2.0) (Brodzik & Knowles, 2002) which was selected for the 3 MO product has also a spatial sampling closer to the sensor nominal resolution.

2.2 Orbit selection

The selection of orbits is needed to filter TBs at high latitudes where a sub-daily revisit is available and to generate the time series dataset on the EASE-Grid 2.0 as input to the MO retrieval. The following criteria are applied for the selection of revisits:

- Ascending and descending orbits are processed separately, since the impact of RFI (Oliva et al., 2012) and sun corrections (Khazaal et al., 2016) between ascending and descending orbits are very different.
- TB products are generated from the snapshot based L1B products which are TBs in the Fourier domain. This consists in an Inverse Fast Fourier Transform (IFFT) to make the transition from the Fourier domain to the spatial domain using the L3 EASE-Grid 2.0. In a subsequent step, TBs measurements corresponding to the same grid point are selected from the different snapshots (for a given grid point, the incidence angle of the observation is different for each snapshot) to construct a grid-point-based product similar to the ESA L1C TB product but in EASEv2 grid. The alternative of interpolating the ESA L1C TB dataset from the 15 km Icosahedral Snyder Equal Area (ISEA) grid to the 25km EASE-Grid 2.0 grid. This option was excluded because it can generate interpolation artefacts on the TB products that would have propagated through the processing chain.
- TB products are filtered at high latitudes where more than one revisit per day occurs (latitudes above 60°N and 60°S). A maximum of one revisit per day is considered. The selection criterion is the minimum distance from the centre of the swath because the radiometric accuracy and resolution is best at the centre. This criterion is applied for each grid node individually.

Earth Syst. Sci. Data Discuss., doi:10.5194/essd-2017-1, 2017
Manuscript under review for journal Earth Syst. Sci. Data
Discussion started: 10 February 2017

At this level the acquisitions for a given day for ascending and descending orbits are separately stored in a 3 dimensional matrix accounting for snapshots, longitude and latitude. A snapshot is an image associated to the acquisition of SMOS during a given integration time (epoch). Snapshots have different epochs and polarization following a preprogramed acquisition sequence. From this product a fixed angle binned TB product is generated as presented in Section 3. The product is also used in the next processing steps of L3SM MO.

- For each retrieval and over each node a 7-days period is considered in which 3 revisits are selected when more are available. The first coincides with the central date (date of main product). The two others correspond to selected dates either before (previous 3.5 days) or after (3.5 days posterior) the considered date. Like in the previous processing step, the selection is done based on minimum distance from the swath centre for each node.

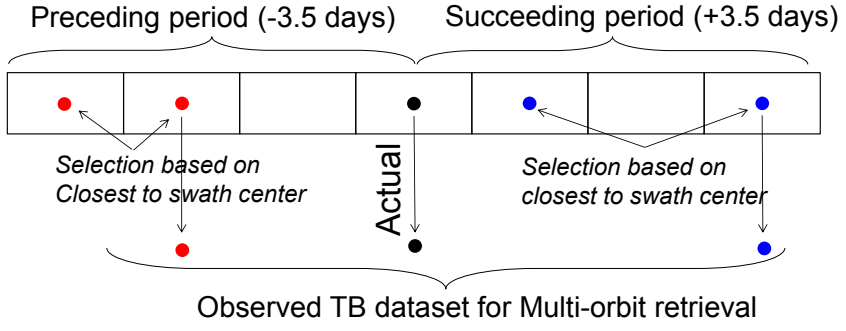

Figure 2 - Selection of revisit orbits for the multi-orbit retrieval at SMOS CATDS.

2.3 Cost function and retrieval

Observed TB at antenna reference frame from the "precedent", "actual" and "succeeding" dates are assembled for each node. The forward algorithm is run to generate the modelled TB for each of the TB dataset records. The ancillary data and parameters are considered for each record independently. A Bayesian cost function that includes the aforementioned MO data, namely observed and modelled TB, is then constructed. This is achieved by incorporating in the retrieval approach a temporal auto-correlation function for the VOD. The cost function is as follows:

Earth Syst. Sci. Data Discuss., doi:10.5194/essd-2017-1, 2017
Manuscript under review for journal Earth Syst. Sci. Data
Discussion started: 10 February 2017

$$Cost = (TB_M - TB_F)^t \cdot \boldsymbol{COV_{TB}^{-1}} \cdot (TB_M - TB_F) + \sum_p (P - P_0)^t \cdot \boldsymbol{COV_p^{-1}} \cdot (P - P_0) \quad (1)$$

Where $\boldsymbol{COV_{TB}} = \sigma_{TB}^2$ is the error covariance matrix of TB data by assuming no auto-temporal correlation, TB_M is the measured TB from SMOS, TB_F is the forward modelled TB using L-MEB, P is the retrieved parameters (SM,VOD), $\boldsymbol{COV_p}$ is the error covariance matrix for parameter P. P_o is the a-priori value of parameter P.

It is important to note that three SM values are retrieved simultaneously at each node: SM_P for the preceding date, SM_A for the actual date and SM_F for the succeeding date. The same applies to VOD. In the case of SM, the a-priori values are given from ECMWF reanalysis data.

When P = SM_P, SM_A or SM_F, the error covariance matrix considering no-cross or auto-correlation is given by:

$$\boldsymbol{COV_{SM}} = \sigma_{SM0}^2 \cdot I \quad (2)$$

where σ_{SM0}^2 is the standard-deviation error associated to SM. It is set to a high value: 0.7 m^3/m^3. **I** is the (3×3) identity matrix.

When P = VOD the error covariance matrix, considering temporal auto-correlation and no-cross correlation between the different parameters is given by:

$$\boldsymbol{COV_{VOD}} = \sigma_{VOD0}^2 \begin{bmatrix} 1 & \dots & \dots \\ \rho(t_P, t_A) & 1 & \dots \\ \rho(t_P, t_F) & \rho(t_A, t_F) & 1 \end{bmatrix} \quad (3)$$

Where σ_{VOD}^2 is the standard-deviation error associated to VOD, and ρ the correlation function modelled assuming a Gaussian auto-correlation distribution:

$$\rho_{VOD}(t_1, t_2) = \rho_{max}(t_1, t_2) \cdot \exp\left(-\frac{(t_1 - t_2)^2}{Tc^2}\right) \quad (4)$$

Where t_1 and t_2 are the time (expressed in days) corresponding to the VOD retrievals dates (P, A or F), $\rho_{max}(t_1,t_2)$ is the maximum amplitude of the correlation function between t_1 and t_2, Tc is the characteristic correlation time for VOD (Tc = 30 days for forests and TC = 10 days for low vegetation).

Earth Syst. Sci. Data Discuss., doi:10.5194/essd-2017-1, 2017
Manuscript under review for journal Earth Syst. Sci. Data
Discussion started: 10 February 2017

252 Figure 3 shows the shape of the correlation function for the two correlation lengths used in the processing.
253 The green curve corresponds to the forested surfaces and the blue one to the nominal surfaces (bare soil
254 and low vegetation).

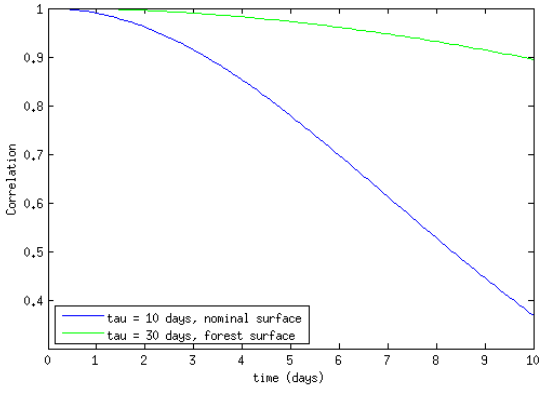

256 *Figure 3 Auto-correlation functions for vegetation optical depth (VOD) for different*
257 *correlation lengths (green: forested surfaces, blue: nominal surfaces).*

258 The parameter values namely (SM_P, SM_A, SM_F, VOD_P, VOD_A and VOD_F) are retrieved by minimising the
259 cost function in an iterative procedure using the Levenberg-Marquardt optimisation algorithm. So, at the
260 end of each daily retrieval, three SM values are available. The retrieval associated to the best goodness of
261 fit (X^2) value is then selected and delivered in the 1 day product. This product is only available when the
262 filtering is finished, and thus with 7 days of lag time. Using the daily maps, time synthesis products (3
263 days, 10 days and monthly) are then provided. A detailed description of the algorithm is presented in the
264 CATDS L3 Algorithm Theoretical Basis Document (Kerr et al.,2013).

265 **3. The CATDS Level-3 angle binned TB processor**

266 The objective of this algorithm is to generate a product containing fixed angle full polarization brightness
267 temperatures at Top of Atmosphere (TOA) but with the polarizations expressed in the ground reference
268 frame (horizontal and vertical components) over the EASE-Grid 2.0. The main input to this algorithm is
269 the dataset of snapshots mentioned in the previous section. The algorithm consists of four steps: (a)
270 filtering, (b) interpolation, (c) reference transformation and (d) angle binning. However note that before
271 being projected to a ground frame, the data is processed in the instrument reference frame. Thus TBs are

Earth Syst. Sci. Data Discuss., doi:10.5194/essd-2017-1, 2017
Manuscript under review for journal Earth Syst. Sci. Data
Discussion started: 10 February 2017

labelled TB_Y and TB_X to express that the polarisations are at satellite level while once processed they will be provided in the ground reference frame and be labelled TB_H and TB_V.

3.1 TB filtering

The filtering eliminates brightness temperatures that are impacted by anthropogenic effects (such as Radio Frequency Interferences (RFI)), or spurious effects (such as sun impact). The filtering criteria, shown in Table 1, are similar to those for L3 MO SM retrieval. All filtering criteria should be met, otherwise the acquisition is discarded. In case a cross-polarisation is discarded, the associated X and Y acquisitions are also removed.

Table 1: List of applied filtering criterion used on brightness temperature products prior to interpolation

Filtering criteria	Applied test	Filtering criteria	Applied test
thresholds	50 K < TB_X & TB_Y < 340 K -50 K < TB_{xy} < +50 K	RFI	L1A STRONG RFI (flag is off)
Amplitude	50 K < $\sqrt{TB_x^2 + TB_y^2}$ < 500 K		L1B STRONG RFI (flag is off)
Standard deviation	TB - 2·ATB < TB < TB +2·ATB		POINT SOURCE RFI (flag is off)
1st Stokes	ST1 – $\overline{ST1}$ < 5 + 4 * ATB		TAILS RFI (flag is off)
Spatial resolution †	SMEF < (55 × 55) km²	Sun correction ‡	SUN_POINT (flag is off)
	LMA / Lmi < 1.5		SUN_TAILS (flag is off)
	BORDER FOV (flag is off)		

Where ATB is the radiometric accuracy of SMOS TB, ST1 is the first Stokes parameter, $\overline{ST1}$ is the average of ST1 over each dwell line (angular signature), ST4 is the forth Stokes parameter, SMEF is the area of the half maximum contour of the mean synthetic antenna pattern, LMA Length of the major axis of synthetic antenna pattern, Lmi Length of the minor axis of synthetic antenna pattern.

† Spatial resolution: eliminates records that are impacted by aliasing (outside the alias free field of view).

‡ if active the flag means that the pixel is located in a zone where a Sun alias was reconstructed (after sun removal, measurement may be degraded). The sun tail is considered when the pixel is located in the hexagonal alias directions centred on a sun alias.

3.2 TB Interpolation

The acquisition sequence of SMOS is shown in Table 2. It shows that at each epoch an acquisition can be co-polarised (X, Y) or combined cross (XY, YX) and co-polarised. The table shows that there is no

Earth Syst. Sci. Data Discuss., doi:10.5194/essd-2017-1, 2017
Manuscript under review for journal Earth Syst. Sci. Data
Discussion started: 10 February 2017

complete dataset at any epoch. A weighted linear interpolation is used to compute the missing acquisitions based on adjacent ones.

Table 2 - Acquisition sequences of SMOS in full polarization mode (capital letters are used for pure acquisition)

Snapshot number	1	2	3	4	5	6	7	8	9	10	11	12
TB (Real/Imaginary)		X/XY		Y/YX		X/XY						Y/YX
TB (co-polarisation)	X	X	Y	y	X	x		Y	X		Y	Y

The weighting function accounts for the two following elements:

- The accuracy of acquisition: the TB acquisitions have different accuracy levels because the integration time is longer when only co-polarisation is acquired (pure acquisition) compared to the case where combined cross and co-polarisation are acquired.

- The time span of acquisition: The time span between two acquisitions of the same mode is not constant. Acquisitions closer in time are considered more reliable than farther ones taking into consideration that the synthetic antenna function is rotating and that the incidence angle is changing.

The time interpolation function of TB at time i (*TBi*) is as follows:

$$\begin{cases} TB_i = \dfrac{W_{i-1}.TB_{i-1} + W_{i+1}.TB_{i+1}}{W_{i-1} + W_{i+1}} \\ W_{i-1} = \dfrac{1}{\sigma_{i-1}.nb\_epo_{i-1}} \\ W_{i+1} = \dfrac{1}{\sigma_{i+1}.nb\_ep_{i+1}} \end{cases} \quad (5)$$

Where nb_epo_i is the number of epochs between acquisitions at time i, σ is the associated radiometric accuracy, W_i is the weighting coefficient at time i. The standard deviation of the interpolated field is computed based on the square root of the weighted variances of the adjacent acquisition. We assume that the acquisitions are not-correlated, therefore no cross correlation term is considered in the equation. The following formulation is used:

$$\begin{cases} \sigma_i = \sqrt{\dfrac{(Q_{i-1}.\sigma_{i-1})^2 + (Q_{i+1}.\sigma_{i+1})^2}{Q_{i-1}^2 + Q_{i+1}^2}} \\ Q_i = \dfrac{1}{nb\_epo_i} \end{cases} \quad (6)$$

Earth Syst. Sci. Data Discuss., doi:10.5194/essd-2017-1, 2017
Manuscript under review for journal Earth Syst. Sci. Data
Discussion started: 10 February 2017

The same approach as eq.(5) while applying a constant weight is used to compute the interpolated values of auxiliary information like major and minor semi-axis length, incidence angle, Faraday angle and geometric angle.

3.3 Transformation from antenna to ground reference frame

In this step, the TBs are transformed from antenna reference frame (X,Y) to the ground reference frame (H,V). This is done without accounting for atmospheric and galactic contributions. They are considered as TOA TBs. The TB components at antenna reference frame exhibit polarisation mixing due to the geometry of the acquisition (Figure 4). Faraday rotation will also alter slightly the polarisations.

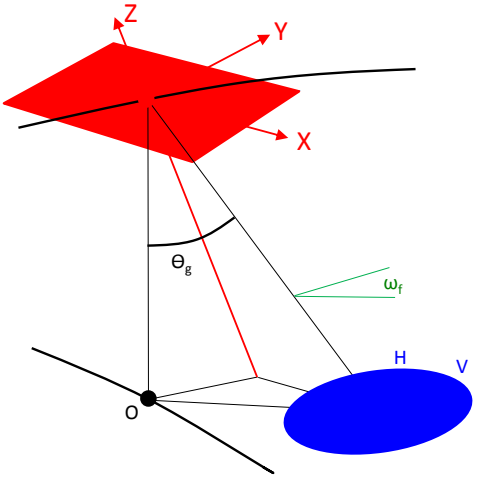

Figure 4 - Transformation from antenna (S) to ground reference frame (G), ω_f is the faraday rotation angle and Θ_g is the geometric rotation angle (adapted from SMOS L2 ATBD).

The inverse of the rotation matrix is used to transform the TB data from antenna to ground reference frame:

$$\begin{bmatrix} TB_H \\ TB_V \\ TB_3 \\ TB_4 \end{bmatrix} = IRM \begin{bmatrix} TB_X \\ TB_Y \\ 2 \cdot reel(TB_{XY}) \\ -2 \cdot imag(TB_{XY}) \end{bmatrix} \quad (7)$$

TB_3 and TB_4 are the Stokes 3 and Stokes 4 components. The Inverse of Rotation Matrix (IRM) is given by:

$$IRM = \begin{bmatrix} \cos^2 a & \sin^2 a & \cos a \,.\, \sin a & 0 \\ \sin^2 a & \cos^2 a & -\cos a \,.\, \sin a & 0 \\ -\sin 2a & \sin 2a & \cos 2a & 0 \\ 0 & 0 & 0 & 1 \end{bmatrix} \quad (8)$$

Earth Syst. Sci. Data Discuss., doi:10.5194/essd-2017-1, 2017
Manuscript under review for journal Earth Syst. Sci. Data
Discussion started: 10 February 2017

Where $a = \Theta_g + \omega_f$ (9)

With Θ_g being the geometric angle and ω_f being the Faraday rotation angle as shown in Figure 4.

The accuracies of the TB data are then computed by propagating the accuracies using the above matrix:

$$\begin{cases} \sigma TBH = \left(IRM_{1,1}^2 \cdot \sigma TB_X^2 + IRM_{1,2}^2 \cdot \sigma dTB_Y^2 + 4 \cdot \left(IRM_{1,3}^2 + IRM_{1,4}^2\right) \cdot \sigma TB_{XY}^2\right)^{0.5} \\ \sigma TBV = \left(IRM_{2,1}^2 \cdot \sigma TB_X^2 + IRM_{2,2}^2 \cdot \sigma dTB_Y^2 + 4 \cdot \left(IRM_{2,3}^2 + IRM_{2,4}^2\right) \cdot \sigma TB_{XY}^2\right)^{0.5} \\ \sigma TB3 = \left(IRM_{3,1}^2 \cdot \sigma TB_X^2 + IRM_{3,2}^2 \cdot \sigma dTB_Y^2 + 4 \cdot \left(IRM_{3,3}^2 + IRM_{3,4}^2\right) \cdot \sigma TB_{XY}^2\right)^{0.5} \\ \sigma TB4 = \left(IRM_{4,1}^2 \cdot \sigma TB_X^2 + IRM_{4,2}^2 \cdot \sigma dTB_Y^2 + 4 \cdot \left(IRM_{4,3}^2 + IRM_{4,4}^2\right) \cdot \sigma TB_{XY}^2\right)^{0.5} \end{cases} \quad (10)$$

Where $IRM_{i,j}$ are the i^{th} column and j^{th} line components of the IRM matrix

3.4 Angle binning

This step consists of averaging the TOA TBs at fixed angle intervals using an arithmetic mean. The selected incidence angle bins, shown in Table 3, are designed to cover also the SMAP acquisition angle (40°).

Table 3 - Selected incident angle bins

Bin id	1	2	3	5	6	7	8	9	10	11	12	13	14
Bin centre	2.5°	7.5°	17.5°	22.5°	27.5°	32.5°	37.5°	40°	42.5°	47.5°	52.5°	57.5°	62.5°
Bin width	5°	5°	5°	5°	5°	5°	5°	5°	5°	5°	5°	5°	5°

All TB values outside the interval defined by mean (TB) ± 2 std (TB), where is the standard deviation of TB for each angle bin (not to be confused with the radiometric accuracy), are considered as outliers and removed from the binning. This helps the removal of the low RFI effects and other undesired impacts. If one component of TB (TB_H,TB_V, TB_{HV}) is filtered out, all the other components are disregarded.

Earth Syst. Sci. Data Discuss., doi:10.5194/essd-2017-1, 2017
Manuscript under review for journal Earth Syst. Sci. Data
Discussion started: 10 February 2017

4. Datasets

4.1 Remote sensing datasets

4.1.1 SMOS CATDS Level 3 soil moisture products

The CATDS Level 3 user data products (CLF3UA/D) are MO soil moisture retrieval products. They contain 1 day global maps of geophysical parameters (SM, VOD, imaginary and real dielectric constant …) computed as described above, processing parameters (percentage of forest cover, type of surface model…) and quality indicators (Probability of RFI, goodness of fit X^2 …) over continental surfaces for ascending and descending orbits separately. They are in the NetCDF format over the EASE-Grid 2.0 25 km. They are generated at the Institut Français de Recherche pour l'Exploitation de la Mer (IFREMER) for CNES and distributed via the CATDS webportal (http://www.catds.fr) and ftp server. The operational production of L3SM started in 2010 and it is currently ongoing. The time span used in this study covers 2010 - 2015 for the global maps and 2010 - 2016 for the time series analysis. The user has access to the latest versions of the products either from reprocessing or from operational processing. The current study uses the latest data corresponding to reprocessing RE04 which uses CATDS V300 corresponding to ESA V620 Level 1 & 2. It is the first simultaneous Level 2 and Level 3 reprocessing campaign since the start of the mission. Previous versions of the L3SM products where compared to soil moisture products from AMSR-E (Al-Yaari et al., 2014 a) and ASCAT (Al-Yaari et al., 2014 b) missions, but this is the first comparison enabling a aligned configuration of the L2SM SO and L3SM MO. It has homogenized inputs (L1B/C) and physical parametrization. It uses the Mironov dielectric constant model (Mialon et al., 2015), enhanced forest parametrization for albedo (Rahmoune et al., 2014), enhanced global soil texture map consistent with the one used for the SMAP mission, and latest RFI detection techniques (Richaume et al., 2014). It uses also the latest (V620) brightness temperature products at Level 1B. The SM maps are extracted in the present study from the L3 product. After extraction, RFI filtering is applied with probability of RFI < 10 % and goodness of fit with a probability of > 0.95.

Earth Syst. Sci. Data Discuss., doi:10.5194/essd-2017-1, 2017
Manuscript under review for journal Earth Syst. Sci. Data
Discussion started: 10 February 2017

366 **4.1.2 SMOS DPGS Level 2 soil moisture product**

367 The ESA L2 Soil Moisture User Data Product (SMUDP), which is a SO retrieval product, is used in this
368 study for comparison purposes. This product is a half-orbit swath based dataset of physical variables (SM,
369 VOD, dielectric constant imaginary and real part…), processing parameters (percentage of forest cover,
370 type of surface model…) and quality indicators (Probability of RFI, X^2, …) over continental surfaces.
371 Ascending and descending orbits are processed separately in the current configuration. The SMUDP
372 product is delivered in the BinX format over the ISEA discrete global grid (Carr et al. 1997), with a
373 hexagonal partitioning of aperture 4 at a resolution of 9 km known as ISEA4H9. The grid point centres
374 have a fixed separation distance of around 15 km. Products are generated at the ESA SMOS Data
375 Processing Ground Segment (DPGS) and disseminated by ESA via Earth Online. The DPGS and CATDS
376 share the same reprocessing dissemination strategy, users are provided access to the most recent
377 products even before the end of reprocessing campaign. Version 620 of SMUDP is used in this study, and
378 the time span selected is 2010-2015 for the global analysis and 2010 – 2016 in the time series analysis.

379 The main characteristics and differences between the L2SM SO retrieval and L3SM MO retrieval
380 products are summarised in Table 4.

381 **4.1.3 SMOS CATDS Level 3 brightness temperature products**

382 The SMOS CATDS full polarisation angle binned daily brightness temperature product (CDF3TA/D)
383 version 310 were downloaded from the same database as the L3 MO SM. These products consist of global
384 1 day maps of full polarisation TB over fixed angle bins with their associated accuracies. Detailed
385 computation was described above in Section 3. The product also contains auxiliary data like the geometric
386 angles, Faraday angles, length of major semi-axis and length of minor semi-axis. Quality flags are also
387 provided in the product. The TB_H and TB_V records are extracted for the 40° bin. No additional filtering is
388 done over these products.

389 **4.1.4 SMAP NSIDC L1C brightness temperature**

390 SMAP mission from NASA was launched in January 2015. It operates like SMOS in L-band using a
391 radiometer and a radar (that was operational for about 80 days). It has a local overpass time at 6H00 am

Earth Syst. Sci. Data Discuss., doi:10.5194/essd-2017-1, 2017
Manuscript under review for journal Earth Syst. Sci. Data
Discussion started: 10 February 2017

and 6H00 pm for ascending and descending orbits respectively but the acquisitions are not necessarily synchronous with SMOS. In this study we use the SMAP TB derived from the radiometer acquisitions. The SMAP L3B_SM_P product is downloaded from the National Snow and Ice Data Centre (NSIDC) website. The SMAP L3 TB is used as input for the SM retrievals and it is corrected for the water contribution and atmospheric effects. It is provided on the EASE 2.0 grid with a 36 km resolution product. The data is in HDF5 format. The TB_H and TB_V records are extracted for year 2015.

Table 4 – Main characteristics of the SMOS Level 3 and Level 2 SM products

Product	L3SM	L2SM
Name of product	MIR_CLF3A/D	MIR_SMUDP
Gridding system	EASEv2	ISEA 4H9
Product sampling	25 km at	15 km fixed
Resolution	*SMOS nominal resolution of 40km*	
Multi-parameter retrieval		Yes
Angular signature		Yes
Polarization impact	yes	Yes
Multi-orbit	yes	No
Forward model	*L-MEB (tau omega)*	
Availability	3.5 - 7 days	6 hours
Processing centre	CATDS (CNES)	DPGS (ESA)
Format	NetCDF	BinX
Version	V300	V620
Coverage	Global grid	Swath based

4.2 *In situ* datasets

In this study, the SMOS soil moisture products are evaluated against two networks with spatially distributed soil moisture data at the footprint scale (USDA Watersheds and AMMA CATCH). The *in situ* soil moisture data from probes installed at near surface are used. These sites provide a soil moisture reading, representative of the first 5 cm of the top soil layer, as they are vertically installed. This may lead to a mismatch between the sensor sampling depth and the expected representative depth 0-2 cm or 0-3 cm of the L-Band microwave radiometers (Escorihuela et al., 2010). The choice of the sites is done to cover

Earth Syst. Sci. Data Discuss., doi:10.5194/essd-2017-1, 2017
Manuscript under review for journal Earth Syst. Sci. Data
Discussion started: 10 February 2017

contrasting environments over two different continents to provide an overview of the SM MO processor performances. The statistics over the sites are computed for data available within 1 hour of space-borne acquisitions (SMOS, SMAP).

4.2.1- AMMA dataset

The AMMA long term observing system (AMMA-CATCH (1996) and AMMA-CATCH (2005)) includes three mesoscale sites located in Niger, Benin, and Mali that are representative of the West-African eco-climatic gradient (Cappelaere et al., 2009; Mougin et al., 2009).. The AMMA-CATCH soil moisture network is a well-established network in terms of satellite product assessment (de Rosnay et al., 2009; Pellarin et al., 2009; Louvet et al., 2015). Niger and Benin, of the three meso-scale sites, are selected for this study. The Niger site, centred at 13.645° N–2.632° E, is mainly composed of tiger bush on the plateaus, fallow savannah and pearl millet crop fields on the sandy slopes (Cappelaere et al., 2009). The Benin site, located at 1.5–2.8° E; 9–10.2° N, is mainly composed of Woody savannah and tropical forest. Most of ground-based instruments are located in the North–West part of the Ouémé catchment (9.745° N–1.653° E). The observed annual rainfall amount was 1578 mm in 2010, 1093 mm in 2011 and 1512 mm in 2012.

4.2.2- USDA - WATERSHEDS

The United States Department of Agriculture (USDA) Agricultural Research Service operates a network of densely instrument watershed across the US. Surface soil moisture (5 cm) is monitored across the watersheds and recorded on an hourly basis since 2002. The USDA provides estimates of the average soil moisture over an area that has approximately the size of a SMOS footprint. Two of the watersheds have been selected for this study: Walnut Gulch (WG), Arizona, USA (Keefer et al., 2008) and Little Washita (LW), Oklahoma, USA (Elliott et al., 1993). Soils in WG can be classified as sandy loam. The original datasets are available from https://www.tucson.ars.ag.gov/dap/ for WG and from http://ars.mesonet.org/webrequest/ for LW. Over LW the soil properties are more heterogeneous with a loam, clay and sand texture. Previous studies on calibration and scaling have quantified the uncertainty of the *in situ* measurements over the sites to be lower than 0.01 m^3/m^3 when compared to gravimetric

Earth Syst. Sci. Data Discuss., doi:10.5194/essd-2017-1, 2017
Manuscript under review for journal Earth Syst. Sci. Data
Discussion started: 10 February 2017

measurements. The basin scale weighted average is based on the Thiessen polygon method and has a standard deviations between 0.05 and 0.10 m^3/m^3. A detailed description of the site characteristics is provided in Jackson et al. (2010), and details on the averaging procedure are provided in Jackson et al. (2012). This network has been used for validation of remote sensing soil moisture datasets (including SMOS) in many studies (Sahoo et al. 2008, Jackson et al. 2012, Leroux et al. 2014). Information on land use and topography of these sites is provided in Table 5.

e 5 – Properties of the in situ sites used for the evaluation

Network (number of stations)	Location	Vegetation/climate	Soil texture	Topography
Walnut Gulch Watershed	Southeastern Arizona, USA	Brush- and grass-covered-Desert shrubs rangeland-Cattle grazing/ Semiarid	Range/sandy loam	Rolling
Little Washita watershed	Southwest Oklahoma, USA	Rangeland and pasture (63%), winter wheat / Sub humid	Range-wheat/silt or sand	Rolling
AMMA Catch network Niger	Niger	South Sahelian climate with semi-arid vegetation and crops (millet, fallows and tiger bush).	sandy loam, 91 % sand and 9% clay	-
AMMA Catch network Ouémé	Benin	Soudanian climate with different types of rain systems and Guinean savanna vegetation.	77% sand and 19 % clay	-

5. Methodology of evaluation

5.1 Global comparison of SMOS and SMAP TB

In order to compare SMOS TB product to SMAP TB, the SMOS daily product was averaged following the same interpolation procedure as the one suggested in the SMAP mission. The method consists in using an inverse distance weighting for all the SMOS EASE 2.0 at 25 km grids point in the limits of the EASE 2.0 at 36 km grid of the SMAP product. The TB_H and TB_V from SMAP product are extracted and used as is. The comparison is done over the pixels with a water fraction of less than 0.001 (i.e. 0.1%) since the SMAP TBs are provided with

racted open surface water.

Earth Syst. Sci. Data Discuss., doi:10.5194/essd-2017-1, 2017
Manuscript under review for journal Earth Syst. Sci. Data
Discussion started: 10 February 2017

449 **5.2 Global Soil moisture maps comparison**

450 Global comparison is done over the EASE-Grid 2.0 25 km used for the L3 MO SM product. The L3 MO
451 SM field is extracted directly from the product. The L2 SO SM product is interpolated to the EASE-Grid
452 2.0 25 km using a three stage interpolation strategy where the availability of the products inside the limits
453 of the grid node is considered:

454 • bilinear, if more than two soil moisture retrievals are available.
455 • linear, if two soil moisture retrievals are available.
456 • nearest point, if one soil moisture retrieval is available.

457 The L2 SO SM is also filtered at high latitude where several soil moisture retrievals are available. The
458 selection criterion is minimum distance from the swath centre, the same as for the L3 MO SM algorithm.

459 **5.2 Local evaluations**

460 No interpolation is used after the extraction of the SM time series. The comparison is based on the
461 following statistical indicators:

462 - Mean bias (m^3/m^3)
463 - Standard Error of the Estimate (SEE) (m^3/m^3)
464 - Pearson correlation coefficient (R)
465 - Root mean square Error (RMSE) (m^3/m^3)

$$RMSE = \sqrt{\frac{1}{N}\sum_{i=1}^{N}(SM_{MO,i} - SM_{SO,i})^2} \quad (4)$$

466 Where $SM_{MO,i}$ is the SM from multi-orbit retrievals and $SM_{SO,i}$ is the SM from single-orbit
467 retrievals.

468 - The empirical cumulative distribution function (Cox & Oakes, 1984).

469 **6. Results & Discussions**

470 **6.1 SMOS and SMAP Brightness temperatures**

471 Figure 5 (a,b) and Figure 6 (a,b) show the comparison between the SMOS L3 TB and SMAP L3 TB at 40°
472 incidence angle. Figure 5 (a) shows the average of SMOS and SMAP TB_H and TB_V for winter (Jan., Feb.,
473 Mar.) and summer (Jul., Aug., Sept.) seasons for year 2016. The gaps (in dark blue) in the SMOS images
474 are due to RFI with a differentiated impact for ascending and descending orbits. The difference in TBs
475 between H/V acquisitions is smaller than between ascending/descending configurations. The SMAP

Earth Syst. Sci. Data Discuss., doi:10.5194/essd-2017-1, 2017
Manuscript under review for journal Earth Syst. Sci. Data
Discussion started: 10 February 2017

products show a higher coverage because SMAP has on-board RFI filtering and mitigation which enables a better coverage but at the cost of a lower radiometric accuracy. The spatial patterns of TB are highly consistent for the two missions. Figure 6 (a,b) show the distribution of difference of TB_H and TB_V from SMOS and SMAP for winter (Jan., Feb., Mar.) and summer (Jul., Aug., Sept.) seasons during year 2016. As described in Section 5.1, only nodes with a water fraction of less than 1 (i.e. 1 %) are considered. The mean difference is about -3.67 K to -4.16 K with SMAP being colder independently of polarization or season. The standard deviation of all comparisons is about 3.65 K. This value is due to differences in calibration of the sensors and to the impact of differences in the acquisition time.

(a) Average three month TB for SMOS and SMAP at H and V polarization for Jan. Feb. Mar.

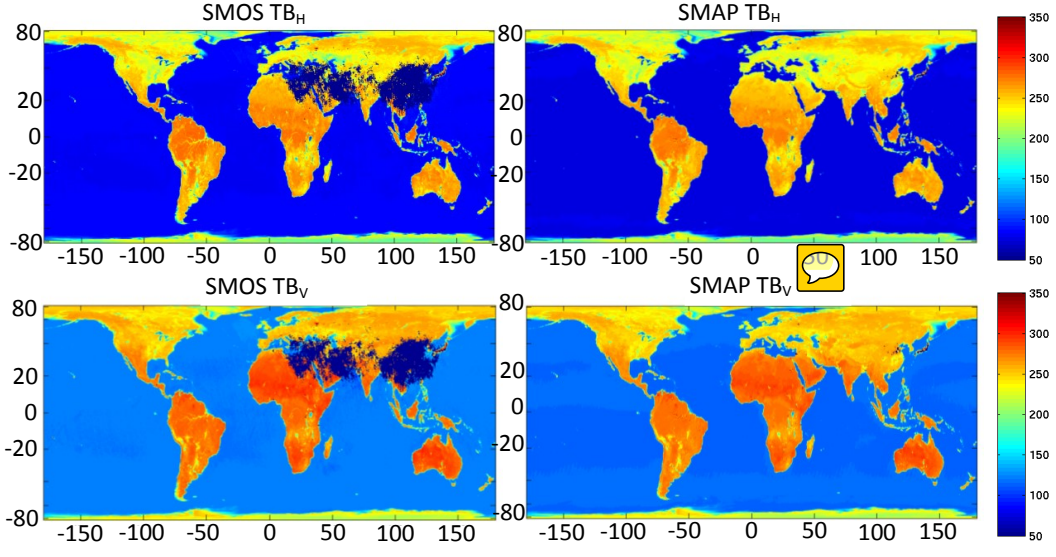

(b) Average three month TB for SMOS and SMAP at H and V polarization for Jul. Aug. Sept.

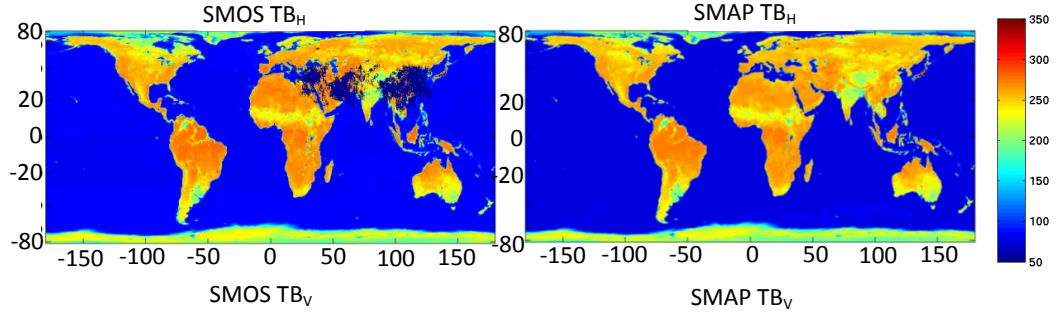

Earth Syst. Sci. Data Discuss., doi:10.5194/essd-2017-1, 2017
Manuscript under review for journal Earth Syst. Sci. Data
Discussion started: 10 February 2017

Open Access Earth System Science Data Discussions

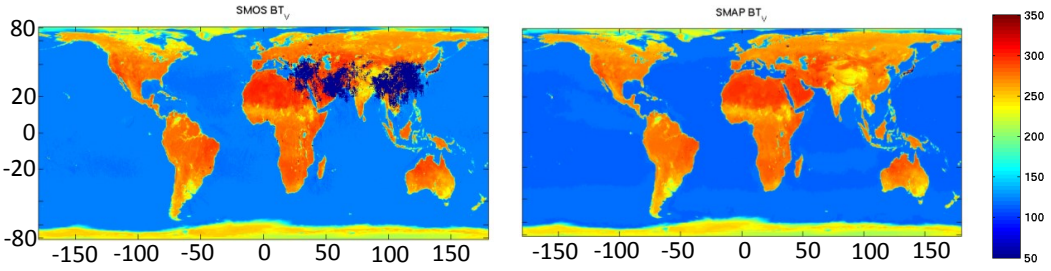

484 *Figure 5 – Three month average maps of SMOS L3 TB @40° (left) and SMAP L3 TB (right) for H*

485 *polarisation, V polarization considering winter: Jan., Feb., Mar. (a) and summer: Jul., Aug., Sept. (b)*

486 *seasons.*

Earth Syst. Sci. Data Discuss., doi:10.5194/essd-2017-1, 2017
Manuscript under review for journal Earth Syst. Sci. Data
Discussion started: 10 February 2017

(a) *Distribution of bias between SMAP and SMOS TB for Jan., Feb., Mar.*

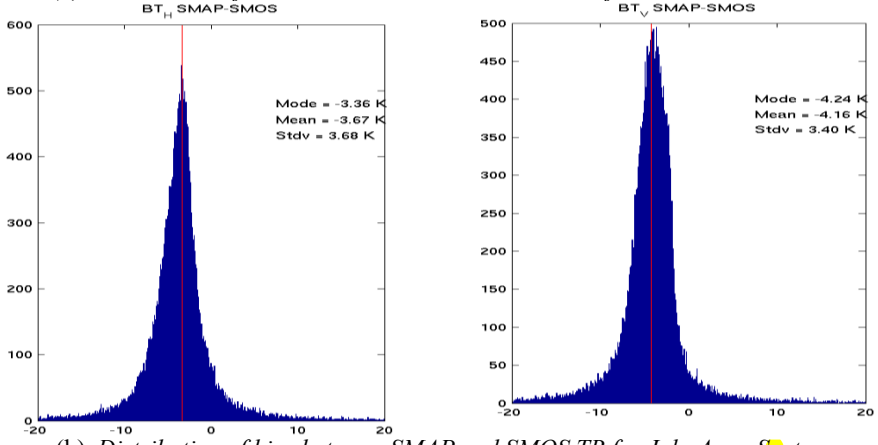

(b) *Distribution of bias between SMAP and SMOS TB for Jul., Aug., Sept.*

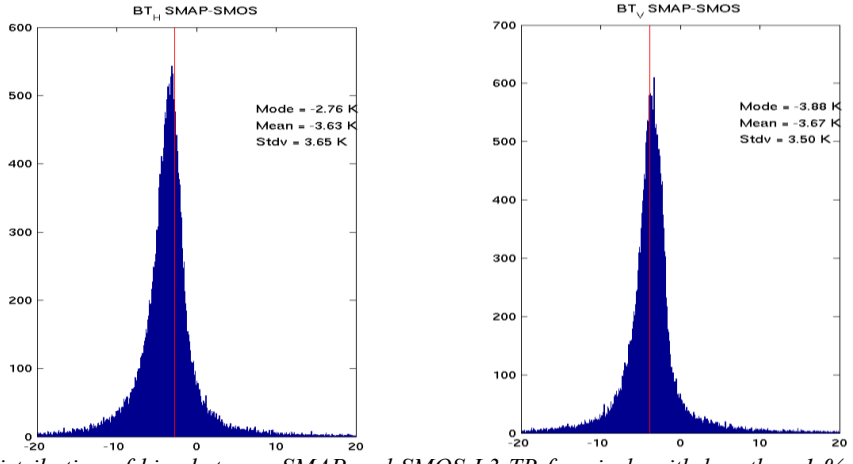

Figure 6 – Distribution of bias between SMAP and SMOS L3 TB for pixels with less than 1 % of water fraction for Jan. Feb. Mar. (a) and Jul. Aug. Sept. (b), H polarisation (right panel) and V polarisation (left panel).

6.2 Soil moisture retrievals at global scale

Based on the aforementioned evaluation methodology the L3SM MO retrievals are compared to those of L2SM SO at global scale over the 2010-2015 period. The auxiliary maps of mean forest cover percentage (Figure 8 a) and average RFI probabilities (Figure 8 b) for year 2011 are provided as complementary information. These maps are obtained from the L3SM product. The mean forest cover (Figure 8 a) provides the percentage of forest cover taking into account the mean antenna pattern. It is obtained by convoluting the ECOCLIMAP (Masson et al., 2003) forest cover by the SMOS antenna weighting function at a resolution of 4 km over an area of 125 × 125 km². The RFI map was obtained by averaging

Earth Syst. Sci. Data Discuss., doi:10.5194/essd-2017-1, 2017
Manuscript under review for journal Earth Syst. Sci. Data
Discussion started: 10 February 2017

498 the RFI probability field in the L3SM product. This information includes strong RFI and moderate RFI
499 depicted from the SMOS full polarization brightness temperatures (Richaume et al., 2014). Some soft and
500 mild RFI are not detected in this product.

501

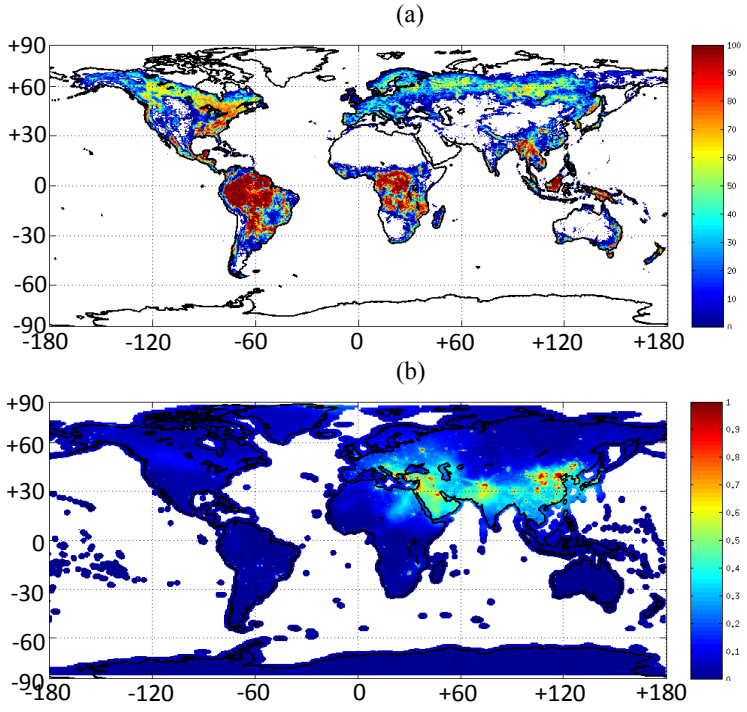

502
503
504

505 *Figure 7 – Global map of the mean forest cover percentage used in the SMOS L2S0 and L3MO soil moisture*
506 *retrievals (a) and map of the Radio Frequency interference (RFI) probabilities (b) for ascending orbit from the*
507 *L3MO soil moisture processor.*

508 Figures 8 (a,b) show the mean number of successful retrievals par year (2010-2015) obtained from L3SM
509 and L2SM respectively. White (Blank) pixels in Figure 8 (a) show the areas where no successful soil
510 moisture retrieval is available. These pixels are mostly located in areas of dense vegetation (Congo), area
511 that are seasonally inundated (Amazon Basin) and/or of high RFI (South-East Asia, Middle-East). From
512 Figures 10 (a) it is clear that the coverage area of the L3SM product is higher in these areas.

513

Earth Syst. Sci. Data Discuss., doi:10.5194/essd-2017-1, 2017
Manuscript under review for journal Earth Syst. Sci. Data
Discussion started: 10 February 2017

514

515

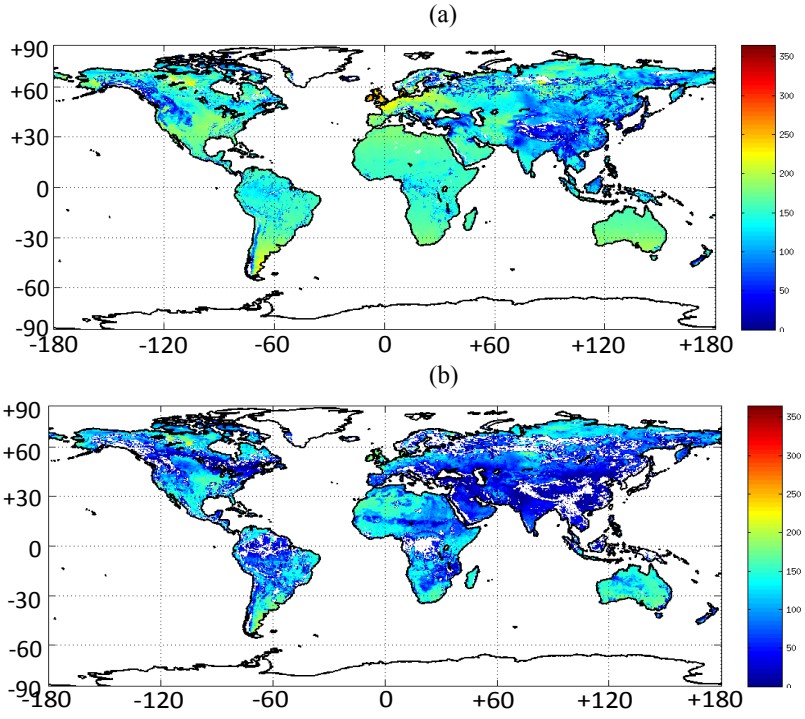

516

517

518

519 *Figure 8* – Mean n*umber of successful SM retrievals per year (2010-2015) for ascending orbits from L3SM-MO (a),*

520 *and L2SM- SO (b).*

521 Figures 9 (a,b) shows the difference (MO-SO) in the number of successful soil moisture retrievals
522 between L3SM and L2SM products. The general behaviour shows a systematic increase in the number of
523 retrievals. The number of retrievals is moderately increasing in desert and plain areas (10-20 retrievals /
524 year / orbits). The increase is much higher for forested areas. The L2SM showed a higher number of
525 successful retrievals in the area between 62°-70° longitude and 35°-55° latitudes. This is due to an
526 anomaly in the processing of TB products. The ancillary data containing the Total Electronic Content
527 (TEC) is not properly used over this region. This has been corrected and all operational products are now
528 properly processed. The archive products will be corrected for this error in the next processing campaign.
529 Also from Figure 13 it is clear that no enhancement in number of retrievals has been observed in areas
530 with very high RFI probabilities in descending orbits (not shown here) like the north Asia region.

531

Earth Syst. Sci. Data Discuss., doi:10.5194/essd-2017-1, 2017
Manuscript under review for journal Earth Syst. Sci. Data
Discussion started: 10 February 2017

532

533 *(a)*

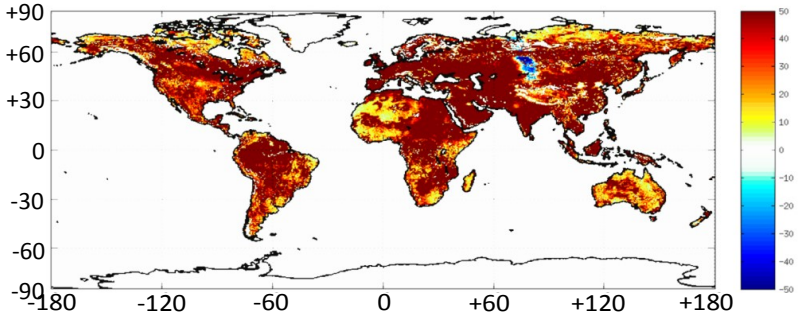

534

535 *(b)*

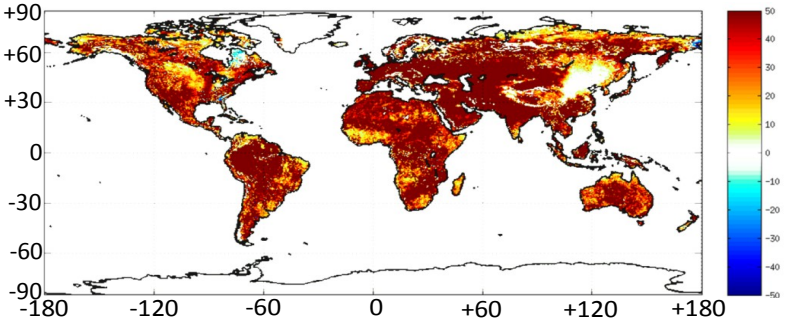

536

537 *Figure 9 – Global map of the difference in the mean number of SM successful retrieval per year over 2011-2015*

538 *($L3SM_{MO}$ - $L2SM_{SO}$) for ascending orbits (a) and descending orbits (b).*

539 The mean soil moisture from L3SM and L2SM for ascending orbits is provided in Figures 10 (a,b). The
540 figures show that the soil moisture spatial patterns are very similar between the SO and MO SM retrievals.
541 The coverage of the multi-orbit product is higher as already shown in the previous figures. Nevertheless
542 some discrepancies can be observed from the difference map (Figure 10 - c). The L3SM MO soil moisture
543 values are generally higher than those of L2SM SO. This is most visible in forested areas (Figure 7 - a)
544 which is consistent with climatic conditions over these areas. It is also higher in areas with high RFI
545 pollution (Figure 7-b). This leads in general to a decrease in the value of the retrieved soil moisture values.
546 So the higher L3SM can be due to the positive impact of using multiple dates during RFI prone periods.

547

Earth Syst. Sci. Data Discuss., doi:10.5194/essd-2017-1, 2017
Manuscript under review for journal Earth Syst. Sci. Data
Discussion started: 10 February 2017

548
549

550

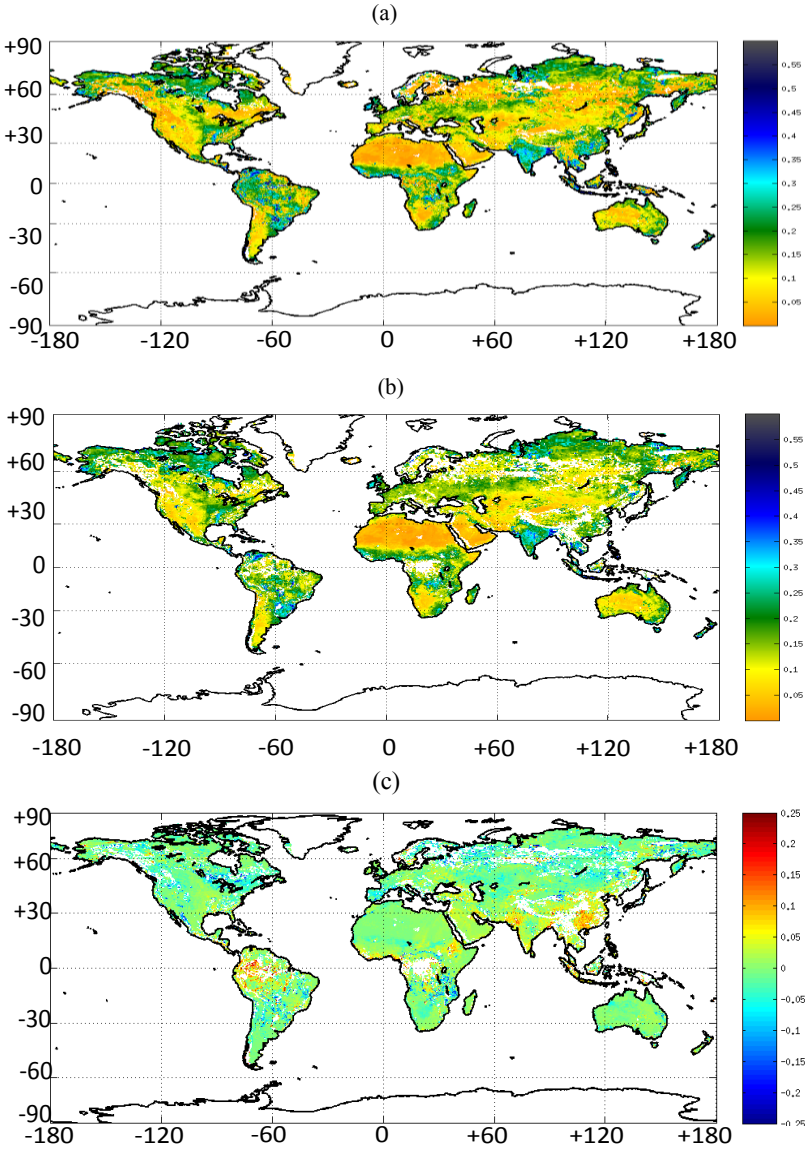

551
552
553
554
555
556
557
558

559 *Figure 10 – Mean soil moisture map over 2011-2015 for ascending orbits from CATDS L3SM MO (a), DPGS L2SM*
560 *SO (b) and the difference (MO-SO) map between L3SM$_{MO}$ and L2SM$_{SO}$ (c).*

561 **6.2 *In situ* comparison**

562 The statistics for the comparison of L2SM SO and L3SM MO with *in situ* networks is shown in Table 3
563 and Table 4 for ascending and descending orbits respectively. The number of retrievals is systematically
564 better for the L3SM than L2SM as expected from the global analysis. Note that, contrary to the global

Earth Syst. Sci. Data Discuss., doi:10.5194/essd-2017-1, 2017
Manuscript under review for journal Earth Syst. Sci. Data
Discussion started: 10 February 2017

analysis, the *in situ* analysis is done without any grid interpolation by considering the closest node. The skills are of similar magnitude for the LW and Niger sites and the lowest skill is obtained for the Benin site in descending overpasses. No site showed lower number of successful retrievals for L3SM than The bias values are not much improved by the L3SM. On the contrary they seem to increase in the majority of the sites. The correlation values range from 0.65 to 0.88 for the different sites. Increased correlation was found for the L3SM products over the Niger site and slightly over WG in descending overpasses. The majority of the correlation values remain high with L3SM retrieval with no significant difference between L2SM and L3SM.

Table 6 – Statistics of the in situ vs SMOS L3SM and L2SM for ascending orbits

Site	R		Bias (m^3/m^3)		SEE (m^3/m^3)		RMSE (m^3 / m^3)		Nb pt	
	L2	L3	L2	L3	L2	L3	L2	L3	L2	L3
AMMA CATCH										
Benin	0.84	0.74	-0.039	-0.058	0.056	0.082	0.068	0.101	484	552
Niger	0.82	0.81	-0.006	-0.003	0.052	0.047	0.052	0.047	617	644
WATERSHEDS										
Little Washita	0.83	0.82	-0.021	-0.03	0.041	0.045	0.046	0.054	625	636
Walnut Gulch	0.81	0.73	0.005	-0.007	0.038	0.053	0.039	0.053	638	643

Table 7 – Statistics of the in situ vs SMOS L3SM and L2SM for descending orbits

Site	R		Bias (m^3 / m^3)		SEE (m^3 / m^3)		RMSE (m^3 / m^3)		Nb pt	
	L2	L3	L2	L3	L2	L3	L2	L3	L2	L3
AMMA CATCH										
Benin	0.74	0.61	-0.029	-0.037	0.069	0.104	0.075	0.11	636	667
Niger	0.63	0.65	-0.011	-0.008	0.049	0.049	0.05	0.05	540	598
WATERSHEDS										
Little Washita	0.81	0.80	-0.001	-0.012	0.042	0.043	0.042	0.044	333	364
Walnut Gulch	0.69	0.72	-0.019	-0.029	0.047	0.048	0.051	0.056	327	360

More in-depth analysis can be obtained by inspecting the times series of soil moisture. Figures 11 and 12 show the time series for the selected sites for the period 2010 to 2016 and for ascending and descending overpasses. The Niger and Benin sites present a very pronounced seasonal signal typical of the Sahelian

Earth Syst. Sci. Data Discuss., doi:10.5194/essd-2017-1, 2017
Manuscript under review for journal Earth Syst. Sci. Data
Discussion started: 10 February 2017

577 sites. Over these sites the L3SM shows consistently lower soil moisture than L2SM for high soil moisture
578 values. The L3SM is closer in this case to the site data. The time series for LW show that the SMOS data
579 closely follows the behaviour of the soil moisture dynamics over this site. One of the reasons is that the
580 rainfall events are well separated enabling the remote sensing data to capture the dynamics of physical
581 processes like infiltration and evaporation at coarse scale. Thus the exponential behaviour typical of a
582 drying soil is well depicted.

Earth Syst. Sci. Data Discuss., doi:10.5194/essd-2017-1, 2017
Manuscript under review for journal Earth Syst. Sci. Data
Discussion started: 10 February 2017

Open Access Earth System Science Data Discussions

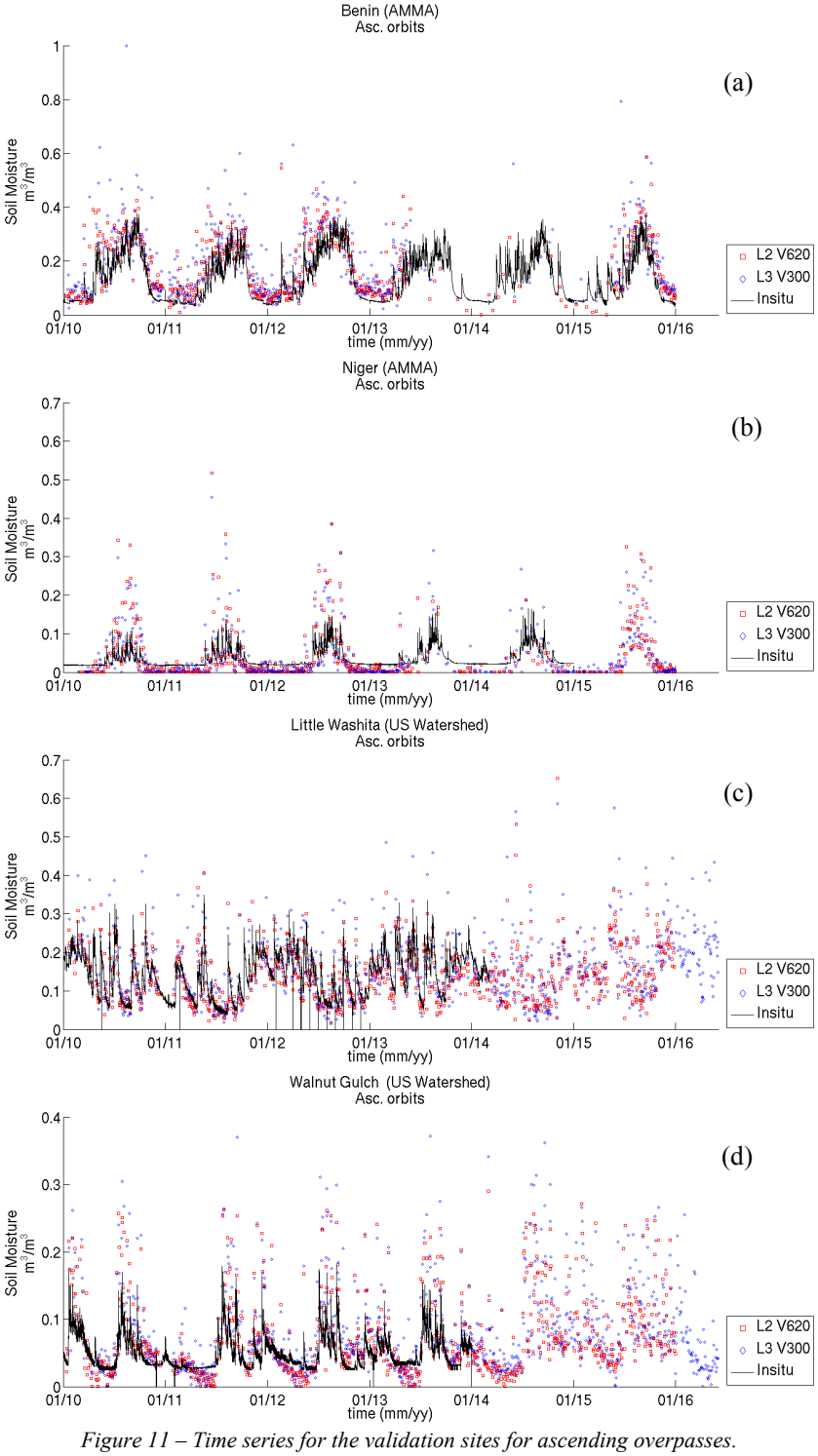

583
584 *Figure 11 – Time series for the validation sites for ascending overpasses.*

585

Earth Syst. Sci. Data Discuss., doi:10.5194/essd-2017-1, 2017
Manuscript under review for journal Earth Syst. Sci. Data
Discussion started: 10 February 2017

Open Access Earth System Science Data Discussions

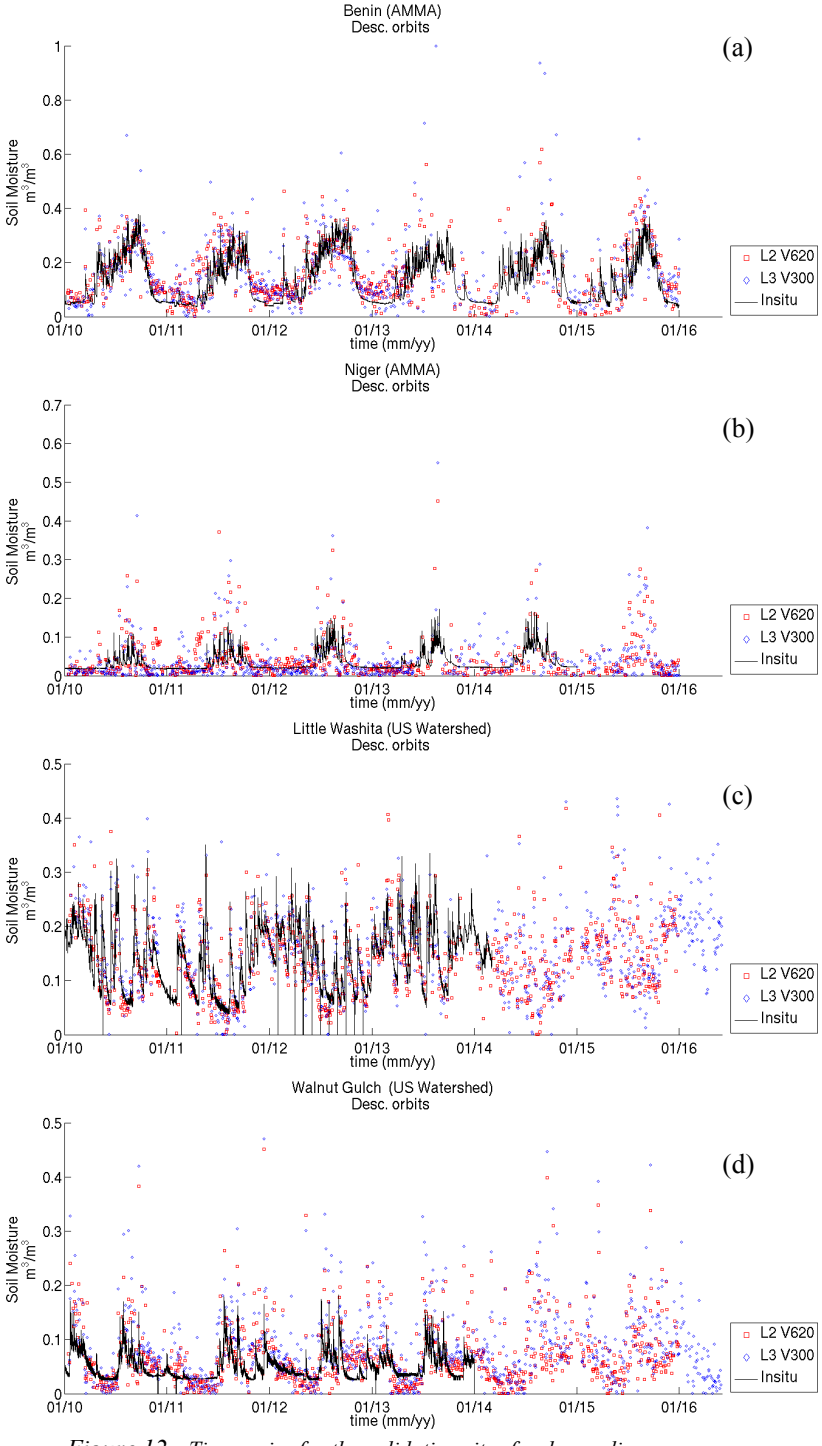

586
587 *Figure 12 - Time series for the validation sites for descending overpasses.*

588

Earth Syst. Sci. Data Discuss., doi:10.5194/essd-2017-1, 2017
Manuscript under review for journal Earth Syst. Sci. Data
Discussion started: 10 February 2017

589
590 Figure 13 and 14 show the CDF of the *in situ*, L2SM and L3SM data for ascending and descending orbits.
591 From these figures it can be concluded that the SMOS soil moisture is drier than the 5 cm *in situ* data
592 across the different values of soil moisture, this can be explained by the SMOS penetration depth with
593 respect to that of ground sensors. Nevertheless the shape of the distribution function, describing the
594 extreme and seasonal cycles, is well captured in most of cases. The Niger site Sahelian climate is well
595 captured with a high probability of low soil moisture values and low number of extreme values. The
596 differences between the L2SM and the L3SM data are mainly observed for the Benin and LW sites. When
597 comparing figure 13 and figure 14 low differences can be notes between ascending and descending orbits.

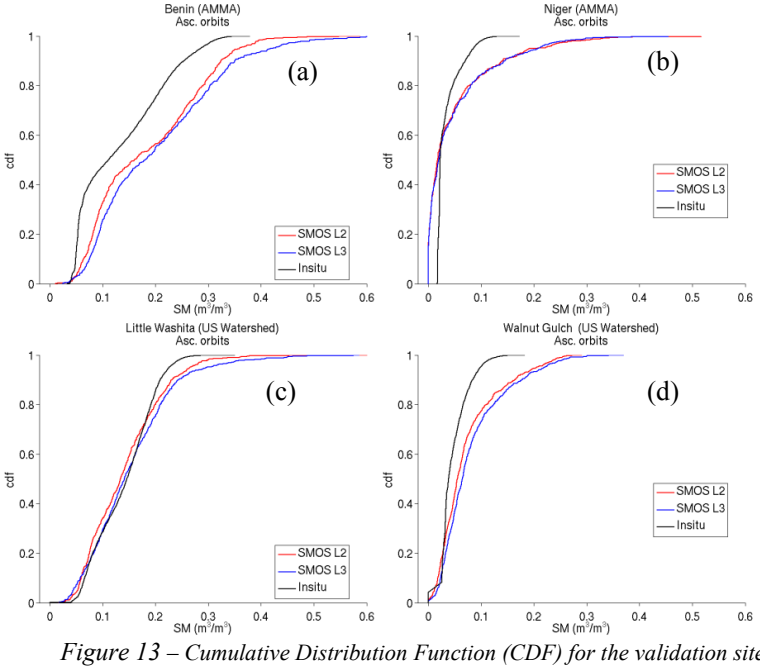

598
599 *Figure 13 – Cumulative Distribution Function (CDF) for the validation sites for ascending overpasses.*

Earth Syst. Sci. Data Discuss., doi:10.5194/essd-2017-1, 2017
Manuscript under review for journal Earth Syst. Sci. Data
Discussion started: 10 February 2017

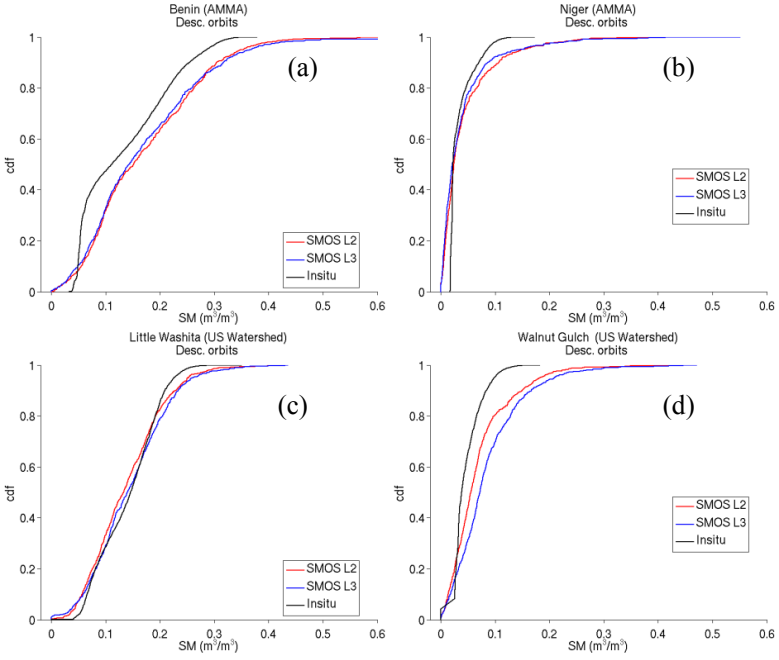

Figure 14 - Cumulative Distribution Function (CDF) for the validation sites for descending overpasses.

7. Conclusions

The level 3 daily maps of soil moisture and brightness temperatures are presented in this paper. A mutli-orbit soil moisture retrieval algorithm for SMOS data is used to obtain the soil moisture product. The main feature of the algorithm is the use of multiple revisits and of auto-correlation of optical vegetation depth in the cost function. The algorithm is implemented operationally at CATDS. The processing chain delivers gridded products over the EASE 2.0 grid at 25 km in NetCDF format. The L3 angle binned TB product is compared to SMAP brightness temperature maps at 40°. The results show small differences in mean TB between the products for H/V polarization and ascending and descending orbits. The SMAP product presents a wider coverage due to the [illegible]oard RFI filtering. The L3 SM product is compared to the L2 SM product. The best improvements in algorithm performances are in terms of the number of successful retrievals observed over forested and RFI prone areas. Also the L3SM product shows on average wetter soil moisture retrievals than L2SM. The comparison with local sites showed that the quality of the retrieval is comparable between L2SM and L3SM. This shows that the increase in the number of successful retrieval does not degrade quality, but rather comes at the expense of an increased time lag in

Earth Syst. Sci. Data Discuss., doi:10.5194/essd-2017-1, 2017
Manuscript under review for journal Earth Syst. Sci. Data
Discussion started: 10 February 2017

product availability (6 hours for L2SM SO versus 3.5 to 7 days for L3SM MO). Future works will concentrate on the associated optical thickness product not presented in this paper. An application of the algorithm to the SMAP data has been envisioned.

Acknowledgements

The SMOS L3SM products were obtained from the Centre Aval de Traitement des Données SMOS (CATDS), operated for the "Centre National d'Etudes Spatiales" (CNES, France) by IFREMER (Brest, France). This study was supported by the CNES “Terre, Océan, Surfaces Continentales, Atmosphère” program. The authors would like to thank the USDA-ARS Hydrology and Remote Sensing Laboratory, AMMA-Catch project for the *in situ* datasets.

References

Al Bitar, A., Leroux, D. J., Kerr, Y. H., Merlin, O., Richaume, P., Sahoo, A., & Wood, E. F. (2012). Evaluation of SMOS Soil Moisture Products Over Continental U.S. Using the SCAN / SNOTEL Network. IEEE Transactions on Geoscience and Remote Sensing, 50(5), 1572–1586.

Al-Yaari, A., Wigneron, J.P., Ducharne, A., Kerr, Y., de Rosnay, P., de Jeu, R., Govind, A., Al Bitar, A., Albergel, C., Muñoz-Sabater, J., Richaume, P. & Mialon, A. (2014a). Global-scale evaluation of two satellite-based passive microwave soil moisture datasets (SMOS and AMSR-E) with respect to Land Data Assimilation System estimates. Remote Sensing of Environment, 149, 181-195

Al-Yaari, A., Wigneron, J.P., Ducharne, A., Kerr, Y.H., Wagner, W., De Lannoy, G., Reichle, R., Al Bitar, A., Dorigo, W., Richaume, P. & Mialon, A. (2014b). Global-scale comparison of passive (SMOS) and active (ASCAT) satellite based microwave soil moisture retrievals with soil moisture simulations (MERRA-Land). Remote Sensing of Environment, 152, 614-626

AMMA-CATCH (1996): Rivers flow and water electrical conductivity, Oueme meso site, Benin. IRD - CNRS - OSUG - OMP - OREME. doi:10.5072/AMMA-CATCH.CL.Run_O

AMMA-CATCH (2005): Surface energy, water vapor, and carbon fluxes, Wankama local site, Niger. IRD - CNRS - OSUG - OMP - OREME. doi:10.5072/AMMA-CATCH.AE.H2OFlux_Ncw

Brocca, L., Melone, F., Moramarco, T., Wagner, W., Naeimi, V., Bartalis, Z., & Hasenauer, S. (2010). Improving runoff prediction through the assimilation of the ASCAT soil moisture product. Hydrology and Earth System Sciences,14(10), 1881-1893.

Brodzik, M. J. and K. W. Knowles. 2002. EASE-Grid: A Versatile Set of Equal-Area Projections and Grids in M. Goodchild (Ed.) Discrete Global Grids. Santa Barbara, California USA: National Center for Geographic Information & Analysis.

Earth Syst. Sci. Data Discuss., doi:10.5194/essd-2017-1, 2017
Manuscript under review for journal Earth Syst. Sci. Data
Discussion started: 10 February 2017

649 Cappelaere, B., Descroix, L., Lebel, T., Boulain, N., Ramier, D., Laurent, J.-P., Favreau, G., Boubkraoui,
650 S., Boucher, M., Moussa, I. B., Chaffard, V., Hiernaux, P., Issoufou, H. B. A., Le Breton, E.,
651 Mamadou, I., Nazoumou, Y., Oï, M., Ottlé, C. & Quantin, G. (2009) The AMMA-CATCH
652 experiment in the cultivated Sahelian area of south-west Niger - Investigating water cycle response
653 to a fluctuating climate and changing environment. Journal of Hydrology, 375. 34–51.

654 Carr D. B., Kahn, R., Sahr, K. & Olsen, T. (1997). ISEA discrete global grids Statist. Comput. Statist.
655 Graph. Newslett., vol. 8, no. 2/3, pp. 31–39.

656 Cox, D. R., & Oakes, D. (1984). Analysis of Survival Data. London: Chapman & Hall.

657 de Rosnay, P., Gruhier, C., Timouk, F., Baup, F.,Mougin, E., Hiernaux, P., Kergoat, L., LeDantec, V.
658 (2009). Multiscale soil moisture measurements at the Gourma meso-scale site in Mali. Journal of
659 Hydrology, 375, 241–252.

660 de Rosnay, P., Drusch, M., Vasiljevic, D., Balsamo, G., Albergel, C., & Isaksen, L. (2013). A simplified
661 Extended Kalman Filter for the global operational soil moisture analysis at ECMWF. Quarterly
662 Journal of the Royal Meteorological Society, 139(674), 1199-1213.

663 Drusch, M. (2007). Initializing numerical weather prediction models with satellite-derived surface soil
664 moisture: Data assimilation experiments with ECMWF's integrated forecast system and the TMI soil
665 moisture data set. Journal of Geophysical Research: Atmospheres, 112(3).
666 http://doi.org/10.1029/2006JD007478.

667 Elliott, R.L., F.R. Schiebe, K.C. Crawford, K.D. Peter and W.E. Puckett. (1993). A Unique Data
668 Capability for Natural Resources Studies. Paper No. 932529, International Winter Meeting;
669 American Society of Agricultural Engineers, Chicago, IL, Dec. 14-17.

670 Entekhabi, D. ,Njoku, E. G., O'Neill, P. E., Kellogg, K. H., Crow, W. T., Edelstein, W. N. ,Entin,
671 J. K., Goodman, S. D., Jackson, T. J., Johnson, J., Kimball, J., Piepmeier, J. R., Koster, R.
672 D., Martin, N., McDonald, K. C., Moghaddam, M. , Moran, S., Reichle, R., Shi, J. C.,
673 Spencer, M. W., Thurman, S. W., Tsang, L. & Zyl, J. V. (2010). The Soil Moisture Active
674 Passive (SMAP) Mission, Proceedings of the IEEE, vol. 98, pp704-716.

675 Escorihuela, M.J., Chanzy, A., Wigneron, J.P., & Kerr, Y.H. (2010). Effective soil moisture sampling
676 depth of L-band radiometry: A case study. Remote Sensing of Environment, 114, 995–1001.

677 Guérif, M., & Duke, C. (2000). Adjustment procedures of a crop model to the site specific characteristics
678 of soil and crop using remote sensing data assimilation. Agriculture, Ecosystems & Environment.
679 http://doi.org/10.1016/S0167-8809(00)00168-7

680 Hagolle, O., Dedieu, G., Mougenot, B., Debaecker, V., Duchemin, B., & Meygret, A. (2008). Correction
681 of aerosol effects on multi-temporal images acquired with constant viewing angles: Application to
682 Formosat-2 images.Remote Sensing of Environment, 112(4), 1689-1701.

683 Hagolle, O., Huc, M., Pascual, D. V., & Dedieu, G. (2010). A multi-temporal method for cloud detection,
684 applied to FORMOSAT-2, VENμS, LANDSAT and SENTINEL-2 images. Remote Sensing of
685 Environment, 114(8), 1747-1755.

686 Hagolle, O., Huc, M., Villa Pascual, D., & Dedieu, G. (2015). A Multi-Temporal and Multi-Spectral
687 Method to Estimate Aerosol Optical Thickness over Land, for the Atmospheric Correction of
688 FormoSat-2, LandSat, VENμS and Sentinel-2 Images. Remote Sensing, 7(3), 2668-2691.

Earth Syst. Sci. Data Discuss., doi:10.5194/essd-2017-1, 2017
Manuscript under review for journal Earth Syst. Sci. Data
Discussion started: 10 February 2017

689 Hollmann, R., Merchant, C. J., Saunders, R., Downy, C., Buchwitz, M., Cazenave, A., ... & Wagner, W.
690 (2013). The ESA climate change initiative: Satellite data records for essential climate
691 variables. Bulletin of the American Meteorological Society, 94(10), 1541-1552.

692 Inglada, J., & Mercier, G. (2007). A new statistical similarity measure for change detection in
693 multitemporal SAR images and its extension to multiscale change analysis. Geoscience and Remote
694 Sensing, IEEE Transactions on, 45(5), 1432-1445.

695 Jackson, T. J., & Schmugge, T. J. (1991). Vegetation effects on the microwave emission of soils, Remote
696 Sensing of Environment, 36(3), 203-212.

697 Jackson T. J., M. H. Cosh, R. Bindlish, P. J. Starks, D. D. Bosch, M. Seyfried, D. C. Goodrich, M. S.
698 Moran, and J. Du. (2010). Validation of Advanced Microwave Scanning Radiometer soil moisture
699 products. IEEE Trans. Geosci. Remote Sens., vol. 48, no. 12, pp. 4256–4272, Dec. 2010.

700 Jackson T. J., Bindlish R., Cosh M., Zhao T., Starks P., Bosch D., Seyfried M., Moran M. S., Goodrich
701 D., Kerr Y. H., and Leroux D. (2012). Validation of Soil Moisture and Ocean Salinity (SMOS) Soil
702 Moisture Over Watershed Networks in the U.S.", IEEE Trans. Geosci. Remote Sens, VOL. 50, NO.
703 5.

704 Jung, M., Reichstein, M., Ciais, P., Seneviratne, S. I., Sheffield, J., Goulden, M. L., ... & Dolman, A. J.
705 (2010). Recent decline in the global land evapotranspiration trend due to limited moisture
706 supply. Nature, 467(7318), 951-954.

707 Keefer, T. O., M. S. Moran, and G. B. Paige (2008), Long-term meteorological and soil hydrology
708 database, Walnut Gulch Experimental Watershed, Arizona, United States, Water Resour. Res., 44,
709 W05S07, doi:10.1029/2006WR005702.

710 Kerr, Y. H., & Njoku, E. G. (1990). Semiempirical model for interpreting microwave emission from
711 semiarid land surfaces as seen from space. IEEE Transactions on Geoscience and Remote Sensing,
712 28(3), 384–393. http://doi.org/10.1109/36.54364

713 Kerr, Y. H., Waldteufel, P., Wigneron, J.-P., Martinuzzi, J. M., Font, J., & Berger, M. (2001). Soil
714 moisture retrieval from space: The Soil Moisture and Ocean Salinity (SMOS) mission. IEEE
715 Transactions on Geoscience and Remote Sensing, 39(8), 1729–1735.
716 http://doi.org/10.1109/36.942551

717 Kerr, Y. H., Waldteufel, P., Wigneron, J.-P., Delwart, S., Cabot, F., Boutin, J., … Mecklenburg, S. (2010).
718 The SMOS Mission: New Tool for Monitoring Key Elements of the Global Water Cycle.
719 Proceedings of the IEEE, 98(5), 666–687. http://doi.org/10.1109/JPROC.2010.2043032

720 Kerr, Y. H., Waldteufel, P., Richaume, P., Wigneron, J.-P., Ferrazzoli, P., Mahmoodi, A., Al Bitar, A.,
721 Cabot, F., Gruhier, C., Enache Juglea, S., Leroux, D., Mialon, A. and Delwart, S. (2012). The
722 SMOS Soil Moisture Retrieval Algorithm. Geoscience and Remote Sensing, 50(5), 1384–1403.

723 Kerr, Y. H., Jacquette, E., Al Bitar, A., Cabot, F., Mialon, A., & Richaume, P. (2013). CATDS SMOS L3
724 soil moisture retrieval processor, Algorithm Theoretical Baseline Document (ATBD).

725 Keyantash, J., & Dracup, J. A. (2002). The quantification of drought: an evaluation of drought indices.
726 Bulletin of the American Meteorological Society,83(8), 1167-1180.

Earth Syst. Sci. Data Discuss., doi:10.5194/essd-2017-1, 2017
Manuscript under review for journal Earth Syst. Sci. Data
Discussion started: 10 February 2017

727 Khazâal A., Anterrieu, E., Cabot, F., Kerr, Y. H. (2016). Impact of Direct Solar Radiations Seen by the
728 Back-Lobes Antenna Patterns of SMOS on the Retrieved Images. IEEE Journal of Selected Topics
729 in Applied Earth Observations and Remote Sensing , vol.PP, no.99, pp.1-8.

730 Konings, A. G., Piles, M., Rötzer, K., McColl, K. A., Chan, S. K., & Entekhabi, D. (2016). Vegetation
731 optical depth and scattering albedo retrieval using time series of dual-polarized L-band radiometer
732 observations. Remote sensing of environment, 172, 178-189.

733 Koster, R. D., Dirmeyer, P. A., Guo, Z., Bonan, G., Chan, E., Cox, P., ... & Yamada, T. (2004). Regions
734 of strong coupling between soil moisture and precipitation. Science, 305(5687), 1138-1140.

735 Rodgers L., & Nicewander A., (1988). Thirteen ways to look at the correlation coefficient. The American
736 Statistician, 42(1), 59–66.

737 Lievens, H., Tomer, S. K., Al Bitar, A., De Lannoy, G. J. M., Drusch, M., Dumedah, G., Franssen, H.J.H.,
738 Kerr, Y. H., Martens, B., Pan, M. and Roundy, J. K. (2015). SMOS soil moisture assimilation for
739 improved hydrologic simulation in the Murray Darling Basin, Australia. Remote Sensing of
740 Environment, 168, pp.146-162.

741 Leroux D. J., Kerr Y. H., Al Bitar A., Bindlish R., Jackson T., Berthelot B., and Portet G. (2014).
742 Comparison Between SMOS, VUA, ASCAT, and ECMWF Soil Moisture Products Over Four
743 Watersheds in U.S., IEEE Transactions on Geoscience and Remote Sensing, VOL. 52, 3.

744 Liu, S. F., Liou, Y.-A., Wang, W. J., Wigneron, J. -P., & Lee, J. B. (2002). Retrieval of crop biomass and
745 soil moisture from measured 1.4 and 10.65 brightness temperatures. IEEE Transactions on
746 Geoscience and Remote Sensing, 40(6), 1260–1268

747 Louvet S., Pellarin T., Al Bitar A., Cappelaere B. Galle Sylvie, Grippa M., Gruhier C., Kerr Y., Lebel T.,
748 Mialon A., Mougin E., Quantin G., Richaume P., & de Rosnay P. (2015) SMOS soil moisture
749 product evaluation over West-Africa from local to regional scale, Remote Sensing of Environment,
750 Volume 156, January 2015, Pages 383-394, ISSN 0034-4257,
751 http://dx.doi.org/10.1016/j.rse.2014.10.005.

752 Masson V., Champeaux J.-L., Chauvin F., Meriguet C., & Lacaze R. (2003) A Global Database of Land
753 Surface Parameters at 1-km Resolution in Meteorological and Climate Models, J. Clim., 16,1261-
754 1282, 2003.

755 Mattia, F., Satalino, G., Pauwels, V. R. N., & Loew, A. (2009). Soil moisture retrieval through a merging
756 of multi-temporal L-band SAR data and hydrologic modelling. Hydrology and Earth System
757 Sciences, 13(3), 343-356.

758 Mialon, A., Richaume, P., Leroux, D., Bircher, S., Al Bitar, A., Pellarin, T., ... & Kerr, Y. H. (2015).
759 Comparison of Dobson and Mironov dielectric models in the SMOS soil moisture retrieval
760 algorithm. IEEE Transactions on Geoscience and Remote Sensing, 53(6), 3084-3094.

761 Miernecki, M., Wigneron, J. P., Lopez-Baeza, E., Kerr, Y., De Jeu, R., De Lannoy, G. J., ... & Richaume,
762 P. (2014). Comparison of SMOS and SMAP soil moisture retrieval approaches using tower-based
763 radiometer data over a vineyard field. Remote Sensing of Environment, 154, 89-101.

764 Mo, T., Choudhury, B. J., Schmugge, T. J., Wang, J. R., & Jackson, T. J. (1982). A model for microwave
765 emission from vegetation-covered fields. Journal of Geophysical Research, 87, 11.229–11.237.

Earth Syst. Sci. Data Discuss., doi:10.5194/essd-2017-1, 2017
Manuscript under review for journal Earth Syst. Sci. Data
Discussion started: 10 February 2017

766 Mougin, E., Hiernaux, P., Kergoat, L., Grippa, M., de Rosnay, P., Timouk, F., et al. (2009). The AMMA-
767 CATCH Gourma observatory site in Mali: Relating climatic variations to changes in vegetation,
768 surface hydrology, fluxes and natural resources. Journal of Hydrology, 375, 14–33.

769 Naeimi, V., Scipal, K., Bartalis, Z., Hasenauer, S., & Wagner, W. (2009). An improved soil moisture
770 retrieval algorithm for ERS and METOP scatterometer observations. IEEE Transactions on
771 Geoscience and Remote Sensing, 47(7), 1999-2013.

772 Njoku, E. G., & Entekhabi, D. (1996). Passive microwave remote sensing of soil moisture. Journal of
773 Hydrology. http://doi.org/10.1016/0022-1694(95)02970-2

774 Njoku, E. G., Jackson, T. J., Lakshmi, V., Chan, T. K., & Nghiem, S. V. (2003). Soil moisture retrieval
775 from AMSR-E. IEEE Transactions on Geoscience and Remote Sensing, 41(2), 215-229.

776 O'Neill, P., Chan, S., Njoku, E., Jackson, T., & Bindlish, R. (2012). Soil Moisture Active Passive (SMAP)
777 Algorithm Theoretical Basis Document (ATBD). SMAP Level 2 & 3 Soil Moisture (Passive),
778 (L2_SM_P, L3_SM_P). Initial Release, 1,
779 (http://smap.jpl.nasa.gov/files/smap2/L2&3_SM_P_InitRel_v1_filt2.pdf).

780 Oliva, R., Daganzo-Eusebio, E., Kerr, Y. H., Mecklenburg, S., Nieto, S., Richaume, P., & Gruhier, C.
781 (2012). SMOS radio frequency interference scenario: Status and actions taken to improve the RFI
782 environment in the 1400-1427-MHZ passive band. IEEE Transactions on Geoscience and Remote
783 Sensing, 50(5 PART 1), 1427–1439. http://doi.org/10.1109/TGRS.2012.2182775

784 Owe, M., de Jeu, R., & Holmes, T. (2008). Multisensor historical climatology of satellite-derived global
785 land surface moisture. Journal of Geophysical Research: Earth Surface, 113(F1).

786 Pellarin, T., Laurent, J.P., Cappelaere, B., Decharme, B., Descroix, L., & Ramier, D. (2009). Hydrological
787 modelling and associated microwave emission of a semi-arid region in South-western Niger. Journal
788 of Hydrology, 375, 262–272.

789 Rahmoune, R., Ferrazzoli, P., Singh, Y. K., Kerr, Y. H., Richaume, P., & Al Bitar, A. (2014). SMOS
790 Retrieval Results Over Forests: Comparisons With Independent Measurements. Selected Topics in
791 Applied Earth Observations and Remote Sensing, IEEE Journal of, 7(9), 3858-3866.

792 Richaume, P., Soldo, Y., Anterrieu, E., Khazaal, A., Bircher, S., Mialon, A., Al Bitar, A., Rodriguez-
793 Fernandez, N., Cabot, F., Kerr, Y., Mahmoodi, A., "RFI in SMOS measurements: Update on
794 detection, localization, mitigation techniques and preliminary quantified impacts on soil moisture
795 products," Geoscience and Remote Sensing Symposium (IGARSS), 2014 IEEE International , vol.,
796 no.,pp.223,226, 13-18 July 2014 doi: 10.1109/IGARSS.2014.6946397

797 Rodríguez-Fernández, N. J., Aires, F., Richaume, P., Kerr, Y. H., Prigent, C., Kolassa, J., Cabot, F.,
798 Mahmoodir, A., Jimenez, J. C. & Drusch, M. (2015). Soil moisture retrieval using neural networks:
799 application to SMOS. IEEE Transactions on Geoscience and Remote Sensing, 53(11), 5991-6007.

800 Sahoo A. K., P. R. Houser, C. Ferguson, E. F. Wood, P. A. Dirmeyer, and M. Kafatos, “Evaluation of
801 AMSR-E soil moisture results using the insitu data over the Little River Experimental Watershed,
802 Georgia,” Remote Sens. Environ., vol. 112, no. 6, pp. 3142–3152, Jun. 2008.

803 Saleh, K.,Wigneron, J. -P., De Rosnay, P., Calvet, J. -C., & Kerr, Y. (2006). Semi-empirical regressions at
804 L-band applied to surface soil moisture retrievals over grass. Remote Sensing of Environment, 101,
805 415–426.

Earth Syst. Sci. Data Discuss., doi:10.5194/essd-2017-1, 2017
Manuscript under review for journal Earth Syst. Sci. Data
Discussion started: 10 February 2017

806 Tomer, S. K., Al Bitar, A., Sekhar, M., Zribi, M., Bandyopadhyay, S., Sreelash, K., ... & Kerr, Y. (2015).
807 Retrieval and Multi-scale Validation of Soil Moisture from Multi-temporal SAR Data in a Semi-Arid
808 Tropical Region. Remote Sensing, 7(6), 8128-8153.

809 Ulaby, F. T., Dubois, P. C., & van Zyl, J. (1996). Radar mapping of surface soil moisture. Journal of
810 Hydrology, 184(1-2), 57–84. http://doi.org/10.1016/0022-1694(95)02968-0

811 Verhoest, N. E., Troch, P. A., Paniconi, C., & De Troch, F. P. (1998). Mapping basin scale variable source
812 areas from multitemporal remotely sensed observations of soil moisture behavior. Water Resources
813 Research, 34(12), 3235-3244.

814 Wagner, W., Lemoine, G. & Rott, H. (1999). A Method for Estimating Soil Moisture from ERS
815 Scatterometer and Soil Data. Remote Sens. Environ. 70, 191–207.

816 Wagner, W., Hahn, S., Kidd, R., Melzer, T., Bartalis, Z., Hasenauer, S., Figa, J., de Rosnay, P., Jann, A.,
817 Schneider, S., Komma, J., Kubu, G., Brugger, K., Aubrecht, C., Zuger, J., Gangkofner, U.,
818 Kienberger, S., Brocca, L., Wang, Y., Bloeschl, G., Eitzinger, J., Steinnocher, K., Zeil, P. & Rubel,
819 F. (2013). The ASCAT Soil Moisture Product: A Review of its Specifications, Validation Results,
820 and Emerging Applications. Meteorologische Zeitschrift, 22(1), 5-33.

821 Wigneron, J.-P., Calvet, J.-C., de Rosnay, P., Kerr, Y.,Waldteufel, P., Saleh, K., et al. (2004). Soil
822 moisture retrievals from bi-angular L-band passivemicrowave observations. IEEE Transactions on
823 Geoscience and Remote Sensing Letters, 1(4), 277–281.

824 Wigneron, J.-P., Kerr, Y. H., Waldteufel, P., Saleh, K., Escorihuela, M.-J., Richaume, P., … & Schwank,
825 M. (2007). L-band Microwave Emission of the Biosphere (L-MEB) Model: Description and
826 calibration against experimental data sets over crop fields. Remote Sensing of Environment, 107,
827 639–655. http://doi.org/10.1016/j.rse.2006.10.014

828